Geophys. J. Int. (2008) **175,** 116–134 doi: 10.1111/j.1365-246X.2008.03863.x

Radial profiles of seismic attenuation in the upper mantle based on physical models

Fabio Cammarano and Barbara Romanowicz

Berkeley Seismological Laboratory, University of California, 215 *McCone Hall* #4760, *Berkeley* CA 94720-4760, *USA. E-mail: fabio@seismo.berkeley.edu*

Accepted 2008 May 21. Received 2008 May 2; in original form 2008 February 18

SUMMARY

Thermally activated, viscoelastic relaxation of the Earth's materials is responsible for intrinsic attenuation of seismic waves. Seismic observations have been used to define layered radially symmetric attenuation models, independent of any constraints on temperature and composition. Here, we interpret free-oscillation and surface wave attenuation measurements in terms of physical structures, by using the available knowledge on the physical mechanisms that govern attenuation at upper-mantle (<400 km) conditions. We find that observations can be explained by relatively simple thermal and grain-size structures. The 1-D attenuation models obtained do not have any sharp gradients below 100 km, but fit the data equally well as the seismic models. The sharp gradients which characterize these models are therefore not required by the data.

In spite of the large sensitivity of seismic observations to temperature, a definitive interpretation is limited by the unknown effects of pressure on anelasticity. Frequency dependence of anelasticity, as well as trade-offs with deeper attenuation structure and dependence on the elastic background model, are less important. Effects of water and dislocations can play an important role as well and further complicate the interpretation. Independent constraints on temperature and grain size expected around 100 km depth, help to constrain better the thermal and grain-size profiles at greater depth. For example, starting from a temperature of 1550 K at 100 km and assuming that the seismic attenuation is governed by the Faul & Jackson's (2005) mechanism, we found that negative thermal gradients associated with several cm grain sizes (assuming low activation volume) or an adiabatic gradient associated with ∼1 cm grain size, can explain the data. A full waveform analysis, combining the effects on phase and amplitude of, respectively, elasticity and anelasticity, holds promise for further improving our knowledge on the average composition and thermal structure of the upper mantle.

Key words: Composition of the mantle; Elasticity and anelasticity; Surface waves and free oscillations; Seismic attenuation.

1 INTRODUCTION

Imperfections in the crystalline structure of any mineral govern deformation and viscoelastic relaxation (anelasticity) at seismic frequencies. The study of different creep mechanisms and their mutual relevance at given *P–T* conditions (Frost & Ashby 1982; Kohlstedt 2008) is useful to understand the possible physical mechanisms that may also be responsible for seismic attenuation (i.e. at much higher frequencies). Recently, accurate experimental data on shear attenuation for mantle minerals at seismic frequencies (e.g. Jackson *et al.* 2002) are starting to provide a better understanding of such phenomena. A grain boundary sliding mechanism seems compatible with laboratory experiments. Temperature and grain-size dependence for olivine polycrystalline samples have been accurately measured and modelled (Faul & Jackson 2005). Measurements on natural dunite samples, which contain hydrous phases, have been also performed very recently (Aizawa *et al.* 2008). Overall, these experiments indicate the important role of water on seismic attenuation and confirm the predictions based on analogy with rheology (e.g. Karato 2006a). Pressure dependence, represented by activation volume, remains mostly unknown, however.

Within the Earth, viscoelastic relaxation is responsible for dissipation and dispersion of seismic waves or what is commonly referred to as intrinsic attenuation. Seismic attenuation mostly affects the amplitude of the waveforms. However, other effects related to the 3-D elastic structure of the Earth (focusing, scattering) and noise in the data makes it difficult to retrieve information on the intrinsic attenuation structure of the Earth (for a review, see Romanowicz & Mitchell 2008). Nevertheless, observations of attenuation of free oscillations and surface waves provide constraints on the radial (1-D) attenuation profile of the Earth's upper mantle. The available data can be fit with relatively simple models (e.g. Okal & Jo 1990; Widmer *et al.* 1991; Romanowicz 1995; Durek & Ekström 1996; Resovsky *et al.* 2005). All seismic models available (see Fig. 1 for

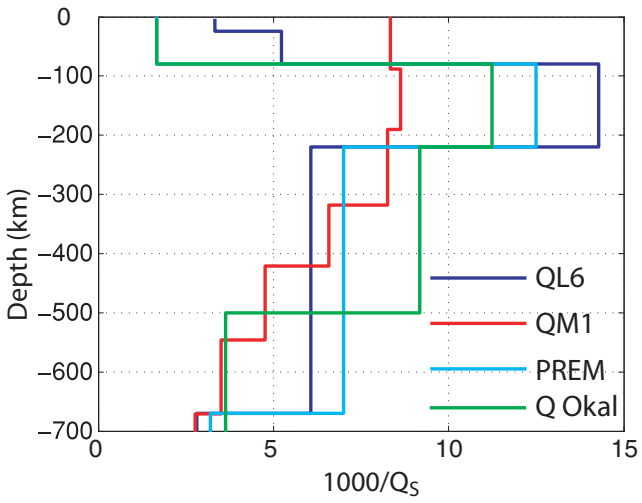

Figure 1. Seismic attenuation 1-D profiles for the upper mantle. QL6 (Durek & Ekström 1996), QM1 (Widmer *et al.* 1991), PREM (Dziewonski & Anderson 1981) and Q Okal (Okal & Jo 1990).

some of them) present a generally similar behaviour in the upper mantle, that is, an increase in attenuation from the top of the upper mantle to the bottom of lithosphere, followed by a sharp decrease just below the lithosphere that tends to become less pronounced with depth. The models are typically represented with layers of uniform attenuation separated by first-order discontinuities. Although convenient, the chosen parametrization hampers a direct physical interpretation of these models. In addition, owing to the non-unique character of any inverse model, it is difficult to assess whether certain features of the seismic attenuation models are actually required by the data. For example, there is much debate about how sharp a decrease in attenuation below the lithosphere is required by the data.

In this paper, we use a different strategy. In the first part, we define directly 1-D attenuation models, based on available constraints from mineral physics and evaluate their fits to seismic normal-mode and surface wave attenuation measurements. For this exercise, we use the pressure, temperature and grain-size dependent model of Faul & Jackson (2005) on dry polycrystalline olivine. A grid search for simple thermal and grain-size structures is performed. In the second part, we assess the role of several physical parameters with the goal of improving the interpretation of global seismic attenuation measurements and to test their actual constraints on the thermal structure of the upper mantle. We document the trade-off between temperature and grain size, based on the Faul & Jackson's model. Effects of water, based on the experimental results from Aizawa *et al.* (2008) and from analogy with rheology, are also tested.

1.1 Temperatures, water and grain sizes in the upper mantle: what is known?

Before discussing the constraints on observed seismic attenuation within the Earth and in the laboratory, it is useful to recall the origin and level of knowledge about upper-mantle temperatures, composition and grain sizes.

1.1.1 Thermal structure

Heat flow measurements place important constraints on the temperature profile of the crust and lithosphere (e.g. Pollack *et al.* 1993). Geothermobarometry studies of xenoliths give information about P–T conditions of the uppermost mantle, helping to constrain lithospheric geotherms (e.g. O'Reilly & Griffin 1987). Both types of data are used to construct geotherms down to the base of the lithosphere. Electromagnetic methods (i.e. resistivity measurements), which are sensitive to even small fractions of partial melt that may occur at the base of the thermal lithosphere, may also help to constrain lithospheric thermal structure (Ledo & Jones 2005). Although different under continents and oceans, lithospheric geotherms are characterized by high thermal gradients, which are compatible with an overall conductive layer. An adiabatic gradient below the lithosphere is expected for the convecting mantle. Potential temperature of the mantle adiabat, based on the temperature needed to generate mid-ocean ridge basalts (MORB), is around 1300 °C (1573 K) at zero depth (McKenzie & Bickle 1988).

Seismic studies are probably the best tool to infer, indirectly, the thermal state of the upper mantle below the lithosphere. Seismic velocities are mostly sensitive to temperature in the upper mantle (e.g. Cammarano *et al.* 2003), although trade-offs with composition and complexities due to phase transitions hamper a clear interpretation. A correct thermal interpretation must account for the dissipative effects due to anelasticity, which determine the non-linearity of $\partial \Delta V_S / \partial T$ (e.g. Karato 1993). Morever, similarly to the attenuation models, seismic velocity models are not required to have a physical meaning. A direct interpretation of seismic data (and not models) in terms of temperature or composition is thus recommended. Although, in this paper, we are concerned with the average thermal structure of the upper mantle, we note that, overall, thermal variations alone can explain a large part of the lateral variations of seismic velocities; however, a secondary compositional signature emerges beneath continents (e.g. Goes *et al.* 2000; Deschamps *et al.* 2002; Cammarano & Romanowicz 2007). To isolate thermal and compositional effects, gravity and geoid data have been used sometimes (Deschamps *et al.* 2001; Forte & Mitrovica 2001) since density varies strongly with composition, whereas temperature variations are dominant for velocity (e.g. Cammarano *et al.* 2003). Direct inversions of seismic data (and not models) for temperature and composition have been recently developed. Previous work on the average structure of the upper mantle (Cammarano *et al.* 2005) found it difficult to fit traveltimes and fundamental modes with an adiabatic pyrolite model. On the other hand, long period waveforms are particularly useful for global studies of the upper mantle. Our previous physical interpretation of these data (Cammarano & Romanowicz 2007) provides robust constraints on the average V_S gradient with depth at mid upper-mantle depths (between 250 and 350 km). The observed gradient would require a negative thermal gradient if composition is assumed to be homogeneous. Alternatively, the gradient can be explained by a gradual enrichment with depth in a more garnet-pyroxene rich (MORB like) composition. Including specific seismic phases, sensitive to the impedance contrast of mantle discontinuities, such as *SS* and *PP* precursors (Cobden *et al.* 2008), may provide additional constraints.

The principal upper-mantle seismic discontinuities, that is, at *ca.* 410 and 660 km, correspond well with the phase transitions olivine to wadsleyite (β- to γ-spinel structure of (Mg,Fe)SiO_2), and ringwoodite (γ-spinel structure) to perovskite + magnesiowüstite. Estimates of temperature, based on experimental phase diagrams of the system Mg_2SiO_4–Fe_2SiO_4 give a temperature of 1760 ± 45 K at 410 km and of 1880 ± 50 K at 660 km (Katsura & Ito 1989; Katsura *et al.* 2004). These values are, overall, consistent with a 1573 K abiabat.

1.1.2 Water

In general, we assume that variations in dry composition do not affect, significantly, the anelastic properties of the upper mantle. However, a trace amount of water in the upper mantle can be present (Hirth & Kohlstedt 1996) and is able to strongly affect the rheological properties of mantle rocks (e.g. Hirth & Kohlstedt 1996; Karato 2006a; Kohlstedt 2008). By analogy, the anelastic properties at seismic frequencies could be affected as well. Elastic properties (e.g. Karato 1995; Jacobsen & Smyth 2006) and mineralogical phase transitions (e.g. Ohtani *et al.* 2004; Litasov *et al.* 2006) are also affected, though the effects on elastic velocities should become significant only around 0.5 wt per cent of water (e.g. Karato 2006b). Geochemical estimates on MORB indicate an amount of water ∼0.1 wt per cent (e.g. Michael 1995). Assuming that MORB is the product of ∼10–20 per cent melting of peridotite (Hirth & Kohlstedt 1996), the primitive mantle rock, thus, should have ∼0.01 wt per cent H_2O, which is distributed between the single mineralogical phases, according to the partition coefficient of each mineral (Hirth & Kohlstedt 1996). In complex tectonic areas and mantle wedges, the amount of water should potentially increase. In the Mediterranean, there is some seismic evidence on presence of water in the upper mantle (e.g. van der Meijde *et al.* 2004), but it is not clear to what extent such a result can be extended globally. Recently, exploiting the strong water sensitivity on attenuation and the relatively small effect on elastic properties compared with the temperature effect (Karato 2006b), it has been possible to infer variations of water content in the upper mantle beneath the northern Philippine sea, by interpreting data of seismic velocity and attenuation (Shito & Shibutani 2003; Shito *et al.* 2006). We do not enter in details on the inversion of 3-D structure here, but we point out that the interpretation, among other factors, is affected by the large uncertainties of material properties at high pressure. In addition, interpretation is further complicated by the non-linearity of the temperature derivatives as a function of temperature, as discussed previously. As a matter of fact, absolute values of seismic velocities are required for a correct interpretation. In summary, although a precise quantification of absolute value of water content is still missing, a (relatively) high water content in mantle wedges seems to be consistent with seismic data (Shito *et al.* 2006).

1.1.3 Grain size

The microstructure of upper mantle rocks contains important information on their deformation history. The grain size of a rock is, indeed, determined by the prevalence of crystal growth compared with other processes such as recrystallization, which tends to reduce the grain size (Derby & Ashby 1987). Deformation mechanisms and grain size are, therefore, strictly related. In general, deformation due to dislocation mechanisms, which is believed dominant at shallow upper-mantle conditions (Karato 1998), is accompanied by recrystallization. Hence, there is a tendency to keep the grain size small. In a regime of diffusion creep, which should govern deformation at higher pressure, grain size can increase. The natural tendency of crystals to grow indefinitely is inhibited because of the polyphase and polycrystalline nature of mantle rocks (Olgaard & Evans 1988). Thus, grain size tends to stabilize.

Petrological information on grain size is limited to relatively shallow depths (down to ∼150 km at the maximum), whereas grain size deeper in the mantle is basically unknown. Also, it may be questioned whether mantle rocks, which arrived at the surface, represent well the characteristics of the rocks *in situ*. Nevertheless, the available constraints on samples and rheological experiments help to put some limits on expected grain size. Textural studies of mantle outcropping and xenoliths (e.g. Lallemant *et al.* 1980) show a large range of grain sizes at sample scale. Variations over more than one order of magnitude, from 0.01 cm to several cm, characterize mantle samples (Boyd & Meyer 1979). At a larger scale, it is generally found that areas that were subjected to major strains, such as collisional areas in the shallow lithospheric mantle, show, on average, smaller grain sizes (Dijkstra *et al.* 2004). Overall, an average diameter of the rock matrix from available upper-mantle samples can be estimated at around 0.1 cm (Boyd & Meyer 1979), though larger diameters, for example, ∼1 cm and more, are not inconsistent with rheology.

1.2 Seismic constraints on attenuation

A seismic wave, propagating within the Earth, loses its energy. Its attenuation is defined as the loss of elastic energy per cycle, that is, $1/Q = \Delta E/2\pi E$, where Q is called the quality factor. Some basic features of attenuation within the Earth have been consistently found, since the first measurements have been performed. Specifically, the measurements of decay of free-oscillation peaks (e.g. Anderson & Hart 1978) and the attenuation with distance of surface waves amplitudes (e.g. Anderson *et al.* 1965) showed that shear attenuation is dominant compared with bulk attenuation (then $Q \approx Q_S$). Furthermore, the comparison of these observations with the attenuation of body waves at high frequency (e.g. Sipkin & Jordan 1979) and of Chandler's wobble at subseismic frequencies (Smith & Dahlen 1981) indicated a weak frequency dependence. The interpretation of the attenuation measurements, as we shall discuss in more detail in the next section, is related to the viscoelastic response of the material and it can be represented by an absorption band model (e.g. Anderson & Minster 1979), where $Q \propto (\omega\tau)^{\alpha}$ being ω the frequency and τ the relaxation time. The frequency dependence α has been estimated to be between 0.1 and 0.4 (for a review, see Romanowicz & Durek 2000). For practical seismological computations, the frequency dependence of attenuation is often ignored ($\alpha = 0$). This simplifies the computations without affecting much the results.

Available compilations of attenuation of surface waves and free oscillations (e.g. Widmer *et al.* 1991; Romanowicz 1995; Durek & Ekström 1996) are collected and distributed on the reference earth model (rem) webpage (http://mahi.ucsd.edu/Gabi/rem.html).

In Fig. 2, we show several compilations of attenuation measurements. Observations of spheroidal and toroidal fundamental modes (respectively, ${}_0S$ and ${}_0T$) are in the top panels, whereas first- and second-order overtones (${}_1S$, ${}_2S$ and ${}_1T$, ${}_2T$) are shown in the bottom panels. The measured free oscillations provide estimates at low harmonic degrees (ℓ) of ${}_0S$ and ${}_0T$ (i.e. long periods) and are sensitive to the global Earth structure. On the other hand, surface waves constrain attenuation at periods below 150 s ($\ell > 60$ for ${}_0S$), which are sensitive to shallow upper-mantle structure. Between 150 and 250 s ($30 < \ell < 60$ for ${}_0S$), attenuation can be estimated with some reliability from both data sets. The origin of the discrepancy between the two data sets (see ${}_0S$ panel) has been discussed and reviewed in several papers (for a review, see Romanowicz & Durek 2000). Most likely, the differences are mostly due to an underestimation of attenuation with free oscillations and an overestimation with surface waves. There is still some controversy, however, about the reliability of one estimate compared with the other. Owing to the very high

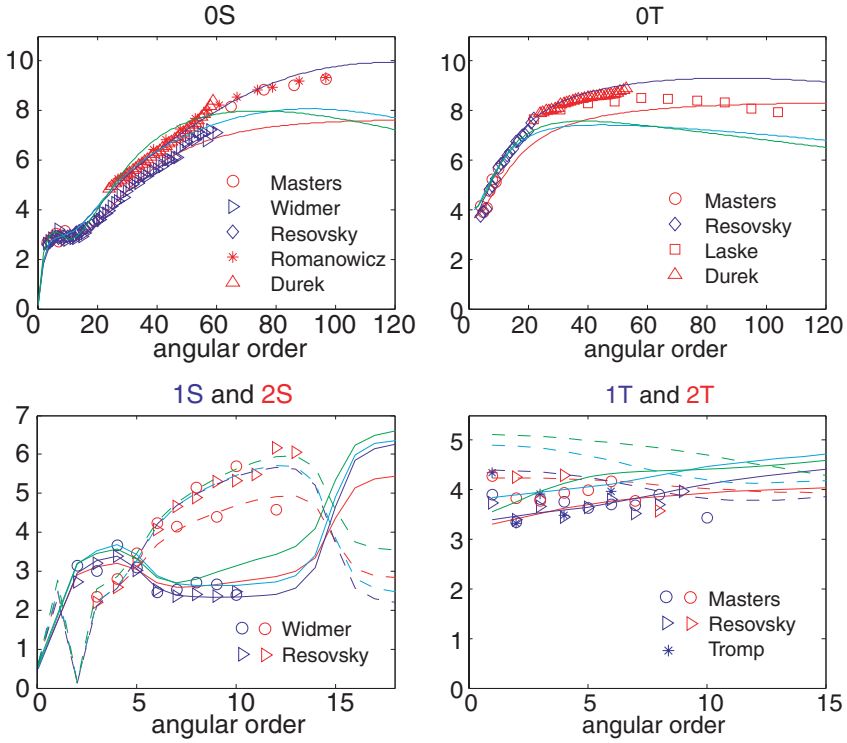

Figure 2. In top panels, compilations of measured attenuation of surface waves (red) and free oscillation (blue), used for spheroidal ($_0S$), toroidal ($_0T$) fundamental modes. Overtones ($_1S$, $_2S$, $_1T$ and $_2T$) are plotted in bottom panels. All data are from REM webpage (http://mahi.ucsd.edu/Gabi/rem.html). Solid lines are predictions for models in Fig. 1 (same colour scheme used before).

sensitivity of attenuation to temperature, we anticipate that such a discrepancy will not affect much the thermal (or grain size) interpretation. The few overtones collected are more sensitive to deeper structure. Some of them provide useful complementary information to fundamental modes for investigating the upper mantle, as we shall see later. Note that overtones have been obtained by using a standing wave approach, and therefore, we expect a bias towards low attenuation when compared with surface wave estimates.

The attenuation measurements as a function of harmonic degree (Fig. 2) are linearly related to the radial profile of attenuation if we assume an elastic, spherically symmetric background model. The partial derivatives (or sensitivity kernels) that link the variations of the data and model are analytically computed, using the classical approach by Woodhouse & Dahlen (1978).

1.3 Mineral physics constraints on attenuation

The viscoelastic (or anelastic) behaviour of a medium subjected to a given stress is, by definition, the observed time-dependent, recoverable strain that follows the instantaneous elastic response and precedes the non-recoverable viscous flow (deformation or creep). The nature of viscoelastic, as well as viscous behaviour of materials, is related to the imperfections that characterize any crystalline medium at thermodynamic equilibrium.

At a given stress level, the mobility of such imperfections cause a delayed (time-dependent) response of the medium. We can express the characteristic relaxation times for a given mechanism as

$$\tau = A\mathrm{e}^{(G^*/RT)}, \tag{1}$$

where A is a constant, G^* is the activation Gibbs free energy, R is the gas constant and T is absolute temperature. G^* can be expressed in terms of activation energy, activation volume and activation entropy as $E^* + PV^* - TS^*$, where the first two terms represent the activation enthalpy (H^*). Ignoring the (small) temperature dependence of entropy and including the activation entropy into the pre-exponential factor, we obtain the typical T dependence of the Arrhenius law. Interestingly, the existing theoretical basis for a physical interpretation of Arrhenius law (kinetic theory of gases and theory of the transition state) have a pre-exponential factor that is slightly T-dependent.

Physical mechanisms such as solid state diffusion of atoms, mobility of linear defects (dislocations) and planar (grain boundaries) are well understood, thermally activated, rheological processes (see Kohlstedt 2008, for a state-of-the-art review on creep mechanisms and their constitutive equation). The role of water, melts and fluids is also being investigated and clarified (see previous paper and Karato 2006a). Similar mechanisms should also be responsible for viscoelastic relaxation at seismic frequencies.

Owing to the inherent difficulty to perform viscoelasticity measurements at seismic frequencies, it has only recently been possible to collect accurate data for mantle minerals. Most of the work has been done by the rock physics group at the Australian National University (ANU), lead by Ian Jackson (Jackson 2008, and references therein). They use a torsional forced-oscillation apparatus (Berckhemer *et al.* 1982; Tan *et al.* 1997; Gribb & Cooper 1998) modified to reach confining pressures up to 0.3 GPa (Jackson & Paterson 1993) to reduce effects due to microcracks and small porespace. The technical details of such instrument and how measurements are performed and samples are prepared, are given in several published papers (see e.g. Jackson 2000; Jackson *et al.* 2002) and they will be not repeated here. The collected measurements allow us to get a first direct look into the mechanisms, responsible for intrinsic seismic attenuation. Faul & Jackson (2005) provide a

rheological model, including elastic, viscoelastic and viscous behaviour, based on 206 measurements of shear modulus and dissipation on polycrystalline (melt-free) olivine. Experiments cover periods between 1 and 1020 s, temperatures from 1000 to 1300 °C and grain sizes from 3 to 165 μm. The Burgers model, used by Faul & Jackson to explain the time-dependent behaviour, is modified to include an absorption band, which accounts for a normalized distribution of relaxation times. An absorption band is consistent with the expected behaviour of natural materials and with seismic observations, as we saw in the previous section. They found a frequency dependence of 0.27 ± 0.01 that is in general agreement with the less constrained, but certainly weak, frequency dependence, observed seismically. A grain-boundary sliding (GBS) mechanism is, overall, consistent with experimental results. A modification of the original physical mechanism proposed by Raj & Ashby (1971), however, seems to be required to correctly reproduce the experimental observations (Faul *et al.* 2004). Specifically, experiments do not identify the transition between the two separate regimes predicted by Raj and Ashby between an elastically accomodated GBS and a subsequent diffusionally accomodated GBS, which involves diffusion along grain boundaries and within grains. Indeed, it seems that the elastically accommodated GBS is precluded in 'pure' melt-free polycrystalline olivine. We refer to Jackson (2008) for a detailed review on the possible physical origins of anelasticity at seismic frequencies. Further discussion on possible alternative physical mechanisms responsible for seismic attenuation at upper-mantle conditions will be given later. We will also model and test the effects of water content, which, as previously mentioned, is an additional but potentially important, parameter.

A mild grain-size sensitivity on Q_S is found in the experiments modelled by Faul & Jackson (exponent is 1.09). Note that the behaviour at coarser grain sizes (>1 cm) and long period (>100 s) is not very well constrained experimentally.

Pressure dependence is not known. We point out that pressure at 100 km is ∼3 GPa and increases to ∼13.5 GPa at 400 km. Reaching such pressures is a major challenge for devices devoted to measure dynamic viscoelasticity. Recently, Li & Weidner (2007) proposed the combined use of multi-anvil high pressure press, with synchrotron X-ray analysis to measure the dynamic response of materials at high P and T. Indirect information on pressure dependence comes again from rheology. Experiments for olivine and other relevant upper-mantle minerals have been performed to relatively high pressures, covering the range expected within the first 400 km. There are, however, still large discrepancies between experiments (e.g. Karato & Jung 2003; Li *et al.* 2006). In addition, it is not guaranteed that the principal mechanism responsible for deformation at upper-mantle conditions is also governing viscoelastic relaxation at the much higher seismic frequencies.

The uncertain value of activation enthalpy at high pressure has justified the adoption of alternative models that assume a constant relation between H^* and the solidus temperature T_S of primitive mantle peridotite rocks. Such an approach takes advantage of the relatively good knowledge of solidus at upper-mantle conditions (e.g. KLB1-N, Hirschmann 2000). This scaling relation, known as Weertman's law, or homologous temperature approach, is expressed as $g = H^*/RT_S$, where the constant g is usually estimated around 30 for the upper mantle (Karato 1993). Note that the pre-exponential factor of the typical Arrhenius law, which describes the P–T dependent attenuation (e.g. Cammarano *et al.* 2003), is not usually determined experimentally. Previous models, such as the ones described in Cammarano *et al.* (2003), used a sort of hybrid approach between a purely mineral physics model and 1-D seismic attenuation models. Namely, the pre-exponential factors are set to obtain values that are consistent with the seismic attenuation models, assuming an adiabatic thermal structure. Such an approach is able to model the P–T dependence of attenuation relatively well but is not informative on the absolute attenuation value at given P–T conditions. For this reason, we will not consider these hybrid models in this paper.

2 MODELLING APPROACH

We use the modified Burgers model defined by Faul & Jackson (2005), and given in the appendix, to predict the shear quality factor (Q_S) for a range of simple thermal and grain-size structures for the shallow upper mantle (down to 400 km). We assume the QL6 (Durek & Ekström 1996) attenuation profile below that depth. Bulk quality factor (Q_κ) is large and does not affect the observations much. We use the large, but finite values of Q_κ from QL6. Tests with the PREM Q model have also been done to estimate the trade-off with deeper (i.e. >400 km) structure. We computed the Q_S values as function of harmonic degree, for fundamental spheroidal and toroidal modes and overtones, assuming a background reference velocity model. To assess how sensitive our results are to the background model used, we tested two alternative velocity models: PREM (Dziewonski & Anderson 1981) and an inverted model from long-period waveforms, named here iPREF (Cammarano & Romanowicz 2007), given in Appendix S1 (supporting information available in the online version of the article) and discussed in a next section. The eigenfunctions of the spherically symmetric model(s) have been computed using the code Yannos (Y. Capdeville, personal communication, 2007; a version of the original MINOS code by Woodhouse 1988). The partial derivatives (or sensitivity kernels) have been computed with the previously mentioned classical approach by Woodhouse & Dahlen (1978).

We compared the predicted values with seismic observations. We used different compilations (see caption of Fig. 2 for references) of measured attenuation of spheroidal and toroidal fundamental modes (${}_0S$ and ${}_0T$) based on attenuation of free oscillations and surface waves. In addition, we also used a few measurements available for first and second overtones (i.e. ${}_1S$, ${}_2S$, ${}_1T$ and ${}_2T$). All the seismic data are taken from the REM webpage.

We defined an L1 misfit function as

$$\frac{1}{N_\ell} \sum_{\ell=1}^{N_\ell} \left| \frac{q_o - q_s}{q_o} \right| \tag{2}$$

and we computed the total misfit for each given structure. We decided to avoid any subjective preference of a data set versus another. In fact, we give the same weight to each data point. As a consequence, regions where few data are available (for example ${}_0T_\ell$ with $\ell > 60$) will have less weight, overall, than better sampled regions of the spectrum. This reflects, in part, the objective amount of knowledge we have at any given point. Furthermore, we do not use the given uncertainties for single measurements. Such uncertainties do not introduce relevant additional information. Indeed, we note that the discrepancy between two different measurements for the same n, ℓ value often exceeds the estimated measurements uncertainties.

Consistent with the frequency of surface waves, we used a reference period of 150 s in the computation of attenuation profiles with the Faul & Jackson model. The frequency dependence determined by their work is $\alpha = 0.27$. Choosing a different period, within the band of surface waves, has a secondary effect on fitting observations compared with the unconstrained pressure dependence, as we shall discuss later.

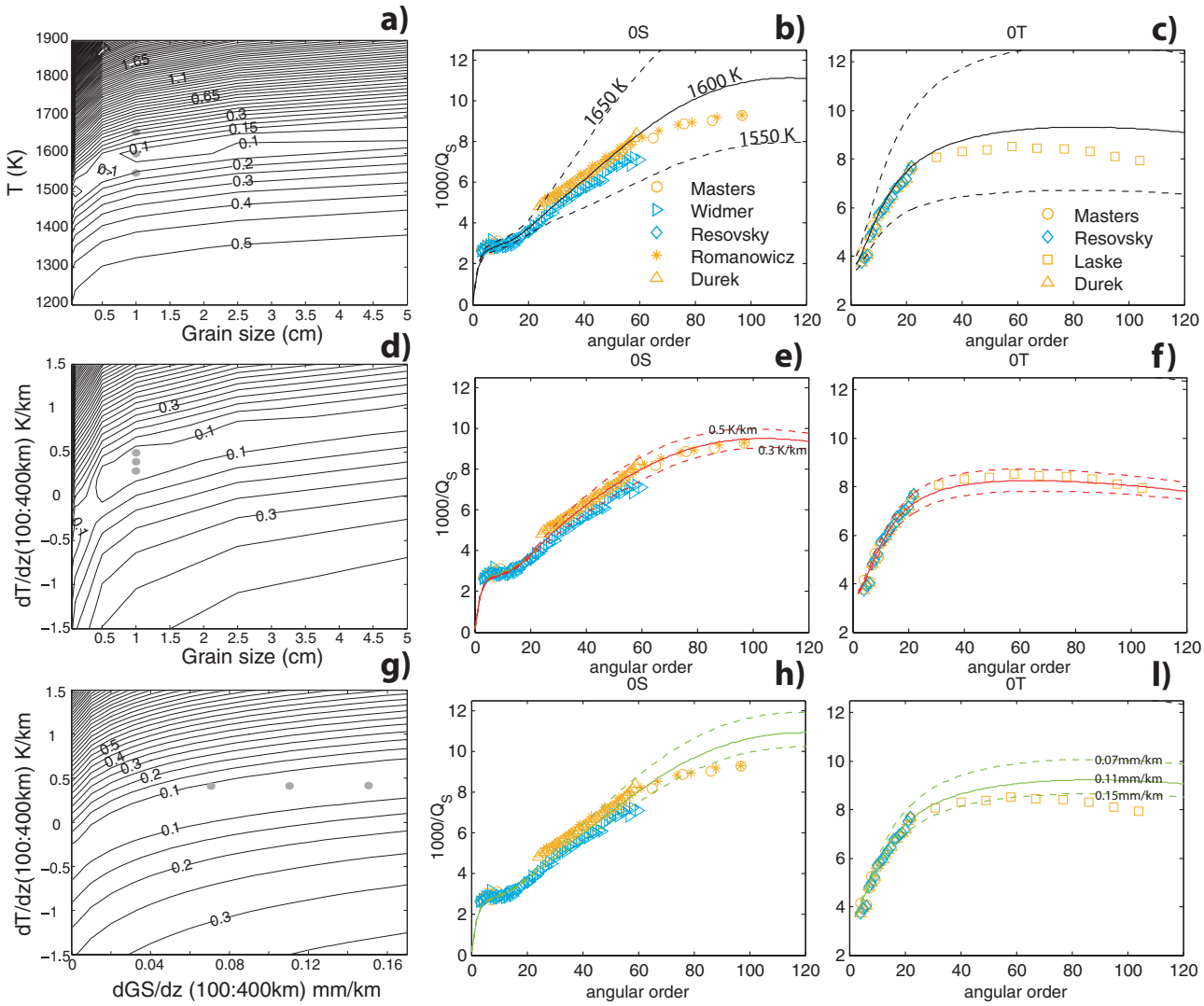

Figure 3. Misfit values for isotherms at constant grain sizes (top panel), for linear thermal gradients between 100 and 400 km, starting from a $T_{\mathrm{REF}} = 1550$ K (middle panel), and for the same thermal structure but allowing grain size to linearly increase from 100 to 400 km starting from a $GS_{\mathrm{REF}} = 1$ mm. Measurements for top and middle panel have been performed at grain sizes of 0.05, 0.1, 0.5, 1, 2.5 and 5 cm every 50 K (top panel) and every 0.1 K km^{-1} (middle and bottom panel). Data for grain-size gradients in bottom panel are every 0.01 mm km^{-1}. Panels on the right-hand side show computed predictions for ${}_0S$ and ${}_0T$ compared with the observations for models represented by grey circles on the left-hand panels. Predictions for overtones are given in the supporting information (Appendix S1). The *P*–*T* and *GS*-dependent model is Faul & Jackson (2005). Reference period is 150 s. V^* is $\sim 12 \times 10^{-6}$ m^3 mol^{-1}. Background elastic model is iPREF (see text).

In what follow, we will first present the results for a set of preferred values of parameters (see caption of Fig. 3). Then, we will show the sensitivity of each parameter. We point out that interpretation is significantly affected by the value of activation volume. In the next section, we used the preferred value of Faul & Jackson (2005), that is, $V^* \sim 12 \times 10^{-6}$ m^3 mol^{-1}. Lacking direct constraints, as discussed earlier, Faul & Jackson chose to tune V^* in their Burgers model to fit both shear velocity and attenuation of 1-D seismic profiles.

3 RESULTS

3.1 Radial attenuation profiles based on physical structures

To highlight the characteristics of the trade-offs between grain size and temperature, we start by computing the misfit values for isothermal structures from 100 to 400 km for various constant grain sizes (Fig. 3, top panel). We assume linear ($\sim$ conductive) thermal gradients for the top 100 km, starting from a temperature of 273 K at the surface and merging with the isotherms at 100 km. Note that the 'cold' structure of the lithospheric part does not affect the measurements significantly. Indeed, we tested that a negligible variation of the misfit pattern is produced when using a common 60 Myr old oceanic geotherm for all thermal structures in the first 80 km, plus a linear gradient in the 20 km below, to join the isotherms. As shown by the contour lines in Fig. 3, Q_S observations are more sensitive to T than grain size. For a given grain size, the average temperature ($\langle T \rangle$) of the upper mantle is potentially very well constrained by seismic observations. For example, with the given parameters listed in the caption of Fig. 3, we found that a 1 mm grain size requires $\langle T \rangle \sim 1500$ K, whereas a 100 K higher temperature is required around 1 cm and slightly increases with coarser grain sizes (Fig. 3a). A variation on the average temperature of ± 50 K greatly affects the

data fit, as shown by the predicted results for the best-fit isotherm, that is, 1600 K, and the 1550 and 1650 K isotherms (Figs 3b and c), at a constant 1 cm grain size. The difference in the prediction of different models is only marginal for ${}_1T_\ell$ and ${}_2T_\ell$ and ${}_1S_\ell$ observations (see Fig. S1 in the supporting information), in agreement with the fact that these modes are relatively insensitive to shallow structure. Only observations of ${}_2S$ with ℓ between 5 and 10 can discriminate between the upper-mantle models. Not surprisingly, larger variations between the models occur for fundamental modes at the highest angular orders. For toroidal modes (Love waves), the discrepancy is already notable at lower ℓ compared with ${}_0S$ (Figs 3b and c), consistent with the shallower depth sensitivity of the former. Even the better isotherm is not able to fit the observations at low and high angular orders simultaneously. Indeed, the 1600 K isotherm provides a good fit for ${}_0S$ and ${}_0T$ until, respectively, $\ell =$ 60 and 50, but the predicted values diverge from observations at higher ℓ (Figs 3b and c). The need to fit ${}_0S$ and ${}_0T$ observations simultaneously, gives additional constraints on the thermal (or grain size) structure required by the *P*-, *T*- and *GS*-dependent attenuation models tested.

In the middle panel of Fig. 3, we show the misfit for thermal structures with linear gradients between 100 and 400 km, at various constant grain sizes. The reference temperature ($T_{\rm REF}$) at 100 km is based on the independent constraints discussed earlier and is fixed at 1550 K, which is consistent with the temperature expected at this depth for a 60 Myr old oceanic geotherm. We find that observations are able to discriminate between different thermal gradients as well. Positive thermal gradients are required at grain sizes around 0.5 cm and larger, whereas negative ones are preferred for millimetre grain sizes. However, only grain sizes around 1 cm ($\pm$0.5 cm) are able to achieve a satisfactory fit, as illustrated in Fig. 4 and discussed later. In Figs 3(e) and (f), we show how predictions change between structures with linear thermal gradients between 0.3 and 0.5 K km^{-1}, and a 1 cm constant grain size. Note that the positive thermal gradients help to obtain the trend in the observations, when moving from low to high angular order.

In Fig. 3(g), we test the same thermal structures, but allowing grain size to linearly increase with depth from 100 to 400 km. We start from a reference grain size, at 100 km, of 1 mm, which is based on the available constraints from petrology. As already discussed before, such an increase is thought to be consistent with the passage from a dislocation controlled deformation regime, which prevents the grain growth because of the dynamic recrystallization, to a diffusive regime, where grains are free to grow. The largest value of the grain size gradient, 0.17 mm Km^{-1}, corresponds to an increase from 1mm at 100 km to 5.2 cm at 400 km. Again, we note that Q_S measurements are less sensitive to grain size than to temperature, as shown by the shape of the contour lines. Based on the physical model (and used parameters) tested, an increase in grain size from mm to cm scale or a large ($\sim$1 cm) constant grain size is required to have a positive thermal gradient, close to an expected adiabatic one (i.e. $\sim$0.4 per cent). However, as illustrated in Figs 3(h) and (l), it is not possible to achieve as good a fit as obtained with the same thermal structure and a constant 1 cm grain size. This is due to the too high attenuation value at 100 km when $T_{\rm REF} = 1550$ K and $GS_{\rm REF} =$ 1 mm. In fact, we obtain a $Q_S \approx 30$, whereas for a $GS_{\rm REF} =$ 1 cm and the same $T_{\rm REF}$, we get $Q_S \approx 50$. Note also that the grain size dependence is becoming less important when moving to coarser grains (Figs 3a, d and g). The behaviour at large grain size, however, is not well constrained experimentally (Faul & Jackson 2005).

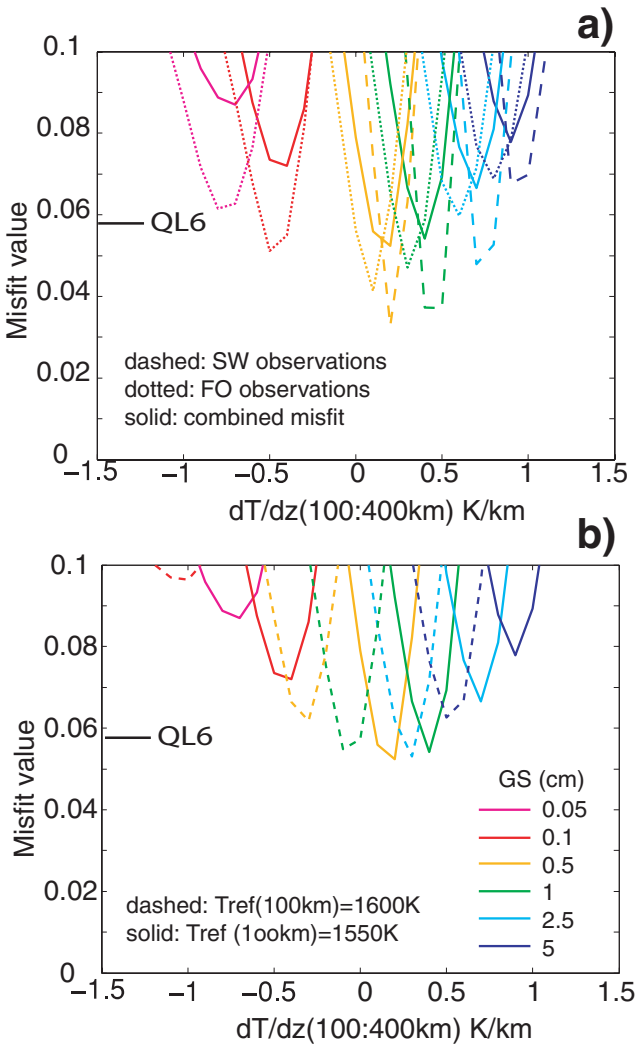

Figure 4. Models with misfit <0.1 for structures in middle, left-hand panel of Fig. 3, plus individual misfit for measured attenuation of surface waves and free oscillations (panel a). Best-fit structures starting from a $T_{\rm REF} =$ 1600 K are on panel b. For reference, the total misfit for the seismic model QL6 is 0.058.

Only some of the models in Fig. 3 obtain an overall misfit <0.1. We can still discriminate within these models and eventually exclude some of them. In Fig. 4, we show the best fits (misfit <0.1) of the physical structures of Fig. 3(d). As already mentioned, if grain size is small, the best fit structures will be characterized by negative thermal gradients, but these structures correspond to a worse fit compared with the positive thermal gradients, associated with larger grain size (Fig. 4a). In the same Figure, we also show misfit values based on separate measurements of surface waves and free oscillations attenuation. The slight variation in the interpretation is due to the discussed difference between the two types of observations at ℓ between 30 and 60 and, more important, to the different coverage, in terms of angular order, between them. This is clearly shown by the shape of the misfit curves in Fig. 5. At the smallest grain sizes (<=1 mm), it is not possible to fit surface wave observations well enough—the computed misfit values are always over 0.1 (out of scale in Fig. 4a). At grain sizes equal to 0.5 and 1 cm, we found thermal structures that are able to fit both data sets well (Fig. 4a). At any given grain size, surface wave

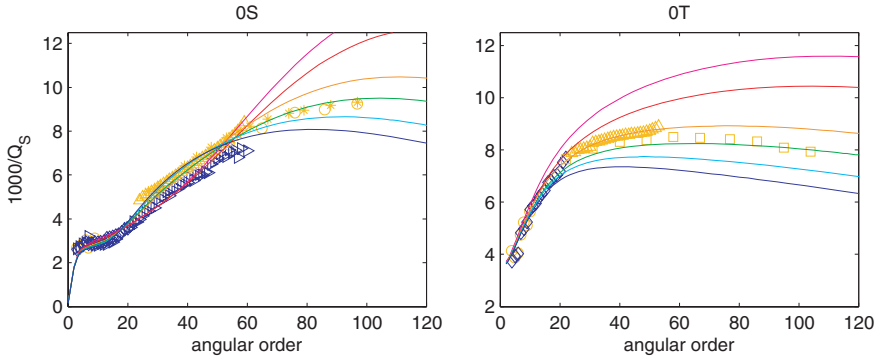

Figure 5. Predictions for fundamental spheroidal ($_0S$) and toroidal ($_0T$) modes for best-fit models of Fig. 4 (solid lines). Colour scheme is the same as on Fig. 4.

observations require a 0.1 K km^{-1} larger thermal gradient compared with free oscillations (Fig. 4a). Note also that the combined misfit at a given grain size is always larger than the one obtained for each single data set. The required thermal gradients will shift towards ∼0.5 K km^{-1} more negative values when starting from a 50 K hotter $T_{\rm REF}$ at 100 km, that is, 1600 K (Fig. 4b). In this case, intermediate grain sizes (around 0.5 cm) are associated with the best-fit thermal structures (Fig. 4b). The opposite is true for a $T_{\rm REF}(100\,{\rm km}) = 1500$ K.

In Fig. 5, we show how the best-fit models represented in Fig. 4(b) (solid lines, that is, for combined misfit) reproduce observations. As already mentioned, a positive thermal gradient helps to obtain the shape required by surface wave observations at high angular orders ($\ell > 30$), whereas the best fit models with negative thermal gradients clearly diverge from observations at very high ℓ.

The depth profiles of three best-fitting attenuation models, based on the physical models in Fig. 3, are shown in Fig. 6 (thick lines). All of them have large attenuation at 100 km. Note, however, that the effect of varying T and GS at this depth is very large. For example,

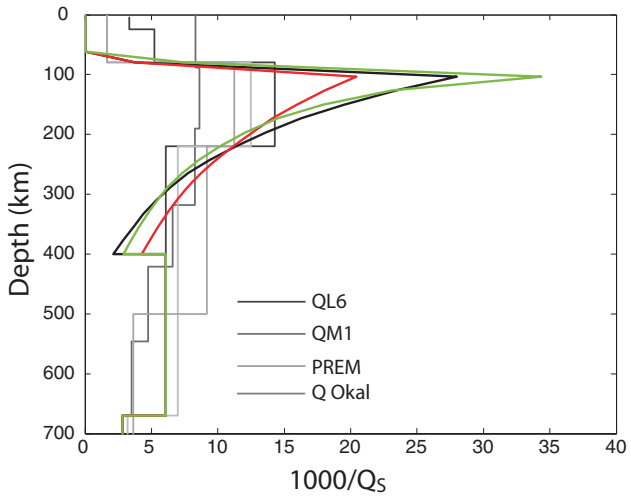

Figure 6. Radial attenuation profiles, based on physical structures. Black is a 1600 K isotherm at constant 1 cm grain size; in red is a $T_{\rm REF}(100\,{\rm km}) = 1550$ K plus a linear thermal gradient of 0.4 K km^{-1} below and 1 cm grain size and, in green, is the same thermal structure but with a grain size that linearly increases from 1 mm at 100 km to 3.4 cm at 400 km. The solid blue model is with $T_{\rm REF}(100\,{\rm km}) = 1550$ K plus a linear thermal gradient of 0.7 K km^{-1} below and 2.5 cm grain size, dashed blue has $T_{\rm REF}(100\,{\rm km}) = 1500$ K plus 0.6 K km^{-1} linear thermal gradient below 0.5 cm grain size. Seismic attenuation models are plotted in background for comparison.

values of 1600 K (black curve in Fig. 6) and 1550 K (red) at 100 km result in attenuation differing by a factor of ∼2. A temperature of 1500 K would produce, for example, a very similar value to QL6 at this depth. Similarly, an increase in grain size would reduce attenuation significantly. Within our search, we indeed found models that have a lower $1/Q$ value around 100 km, overall, more consistent with accurate regional observations (Yang *et al.* 2007). At the same time, they are characterized by a slower decrease in attenuation below. We plot two of them in Fig. 6. These models, however, are not consistent with T or GS structure expected in the upper mantle. A more complete overview on the characteristics of the tested physical models is given in the supporting information.

We would like to stress again that no definitive conclusions should be drawn by such an analysis because of the large uncertainties in the physical attenuation model and because effects of 3-D structure play an important role on average attenuation. Because we rely on a physical mechanism of attenuation for olivine, we prefer to not extend our interpretation into the transition zone. As a consequence, the 1-D models obtained have a jump at 400 km, where they merge with QL6. For the same reasons mentioned above, which we will outline in more detail in the discussion section, one should not be worried about this imposed jump. We may already note, however, that the shape of the models cannot continue its trend below 400 km, without affecting the data fit significantly.

In summary, using a physical model of seismic attenuation, based on mineral physics constraints, it is possible to find relatively simple thermal and grain size structures of the upper mantle, which are able to explain observations of seismic attenuation. Owing to the large uncertainties in some key parameters, such as V^*, the significance of the obtained T and GS structure is tentative. In addition, effects of water and dislocations can also play an important role in the Earth's upper mantle. In the second part of the paper, we will discuss, thoroughly, the sources of uncertainties and their effects on interpretation. It is important to note, however, that the available attenuation measurements contain much more information than what was possible to realize by simply looking at seismic attenuation models. The shape of the physical attenuation models (Fig. 6) does not have any sharp boundaries (except at the base of the conductive lithosphere, fixed at 100 km), which are therefore not required by the global data used. Indeed, the red model in Fig. 6 fits the data similarly to the seismic models (see Fig. 4).

3.2 Constraints on upper-mantle temperatures and grain sizes

In the previous section, we assessed the quantity of information that can be obtained with the available measurements of seismic

attenuation. To do this, we interpreted those data directly in terms of physical parameters, that is, temperature and grain size, by using a *P*-, *T*-, and *GS*-dependent attenuation model, based on laboratory experiments. As a general result, we found that it is indeed possible to fit the seismic observations quite well with simple T and GS structures. In spite of the trade-off between these two parameters, combining the constraints from attenuation observations and from the independent knowledge on expected T and GS at shallow upper-mantle depths, helps to reduce the possible combinations. Nevertheless, the physical interpretation of seismic measurements relies on several assumptions. The first basic assumption is that the mechanism observed in the laboratory experiments, at low pressure and for dry, melt-free polycristalline olivine, is the one which governs intrinsic attenuation in the mantle. Second, we assume that no other effect than intrinsic attenuation (e.g. scattering) affects the observations. We will discuss these two aspects later. In particular, effects of water will be treated separately in the next section.

In this section, we evaluate how interpretation is affected by (a) the deeper (>400 km) attenuation structure, the shallow (<80 km) one and the background elastic model used and, more importantly, (b) the uncertainties on some key mineral physics parameters. Among these, the role of activation volume is certainly the most important. We test the extremely different constant values of V^* that have been used by Faul & Jackson (2005). A reduction of the activation volume with pressure (i.e. depth) is also expected. Estimation of activation volume can be done by using classical elastic strain energy models (Zener 1942; Keyes 1963) or by using the semi-empirical relation with melting temperature proposed by Weertman (1970). The effect is particularly significant for the lower mantle. In general, V^* can decrease by ∼50 per cent from the top to the bottom of the lower mantle (e.g. Sammis *et al.* 1981; Poirier & Liebermann 1984; Matas & Bukowinski 2007).

We test V^* decreasing with pressure (or depth) by using a scaling relation with the elastic model (Poirier & Liebermann 1984):

$$\frac{\partial \ln V^*}{\partial P} = -1/K_S\left[1 + (\gamma)/\left(\gamma - \frac{1}{3}\right)\right], \tag{3}$$

where K_S is the adiabatic bulk modulus and γ is the thermodynamic Grüneisen parameter. The relation is based on the elastic strain energy model, by assuming that all the acoustic modes of the Grüneisen parameter are equal to the thermodynamic Grüneisen parameter (γ). It also assumes that $\gamma\rho$ is constant. Although such assumptions work better with packed structures typical of lower-mantle minerals, the relation gives an idea of the pressure dependence of V^*.

The background elastic model used is derived from a recent average seismic model for the Earth's upper mantle (Cammarano & Romanowicz 2007). In the supporting information, we give the V_P, V_S and density (ρ) table for this model (Table S1; named iPREF). This seismic model is consistent with long-period seismic waveform data and does not have a 220 km discontinuity. K_S is computed as $\rho \times (V_P^2 + \frac{4}{3}V_S^2)$. The thermodynamic Grüneisen parameter

$$\gamma = \frac{\alpha K_S}{\rho C_P} \tag{4}$$

is computed with K_S and ρ from the seismic model, assuming the heat capacity C_P to be 1350 J kg^{-1} K^{-1}, and we let the thermal expansion α decrease linearly from 3.5 × 10^5 to 2.3 × 10^5 K^{-1} between 100 and 400 km. We predict a variation in activation volume of ∼5 per cent from the top reference value at 100 km, which is certainly small, but, in many cases, not negligible. For example, starting from a V^* at 100 km equal to 1.2 × 10^{-5} m^3 mol^{-1} (Faul & Jackson's model preferred value) and assuming a simple T = 1600 K isotherm, we found that Q_S values at 350 km depth are ∼20 per cent lower when the pressure dependence is modelled than in the case when V^* is assumed constant with depth.

3.2.1 Trade-off with lower- and shallow-mantle structure and sensitivity to the background elastic model

To illustrate, in more detail, how the deeper structure affects the physical interpretation in the first 400 km of the upper mantle, we computed the misfit obtained by using the PREM attenuation profile below 400 km, instead of QL6. As expected, overtones (see Fig. S3 in the supporting information) and low angular-order fundamental modes ($\ell < 40$ for $_0S$ and $\ell < 60$ for $_0T$; Fig. 7) are affected by the deeper attenuation structure. Overall, the interpretation does not change much from the one obtained using QL6 (Fig. 8). For all the physical structures in Fig. 8, the best-fit models are slightly worse than for the standard case (named hereafter FJ-150s). This is mostly due to the 'too high' value of attenuation in PREM just below 400 km compared with the value required by the data . Indeed, the jumps at 400 km for all the best-fit models become larger when PREM attenuation, instead of QL6, is used (see Fig. 6). In addition, we note that the thermal gradient required at a given grain size reduces slightly (Fig. 8, bottom panels) to counter-balance the effects on the predictions at low ℓ mentioned above.

In Fig. 8, we also plot the results obtained by using PREM as background elastic model instead of iPREF. Note that using a

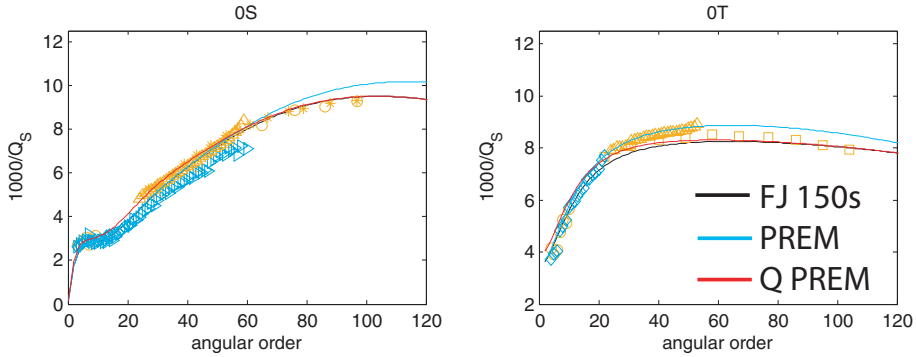

Figure 7. Predictions for $_0S$ and $_0T$ for a thermal structure with a $T_{\rm REF}$(100 km) = 1550 K plus a 0.4 K km^{-1} thermal gradient below and grain size = 1 cm. Black curve (FJ, 150 s) is the regular Faul & Jackson model at a reference period 150 s, light blue (PREM) is using PREM as background elastic model, instead of iPREF, red (Q PREM) is using PREM attenuation profiles, instead of QL6, below 400 km, green (Q TOP) is using an uniform layer with $Q_S = 300$ for the top 80 km instead of the computed lower attenuation. Predictions for overtones are given in Fig. S2 of the supporting information.

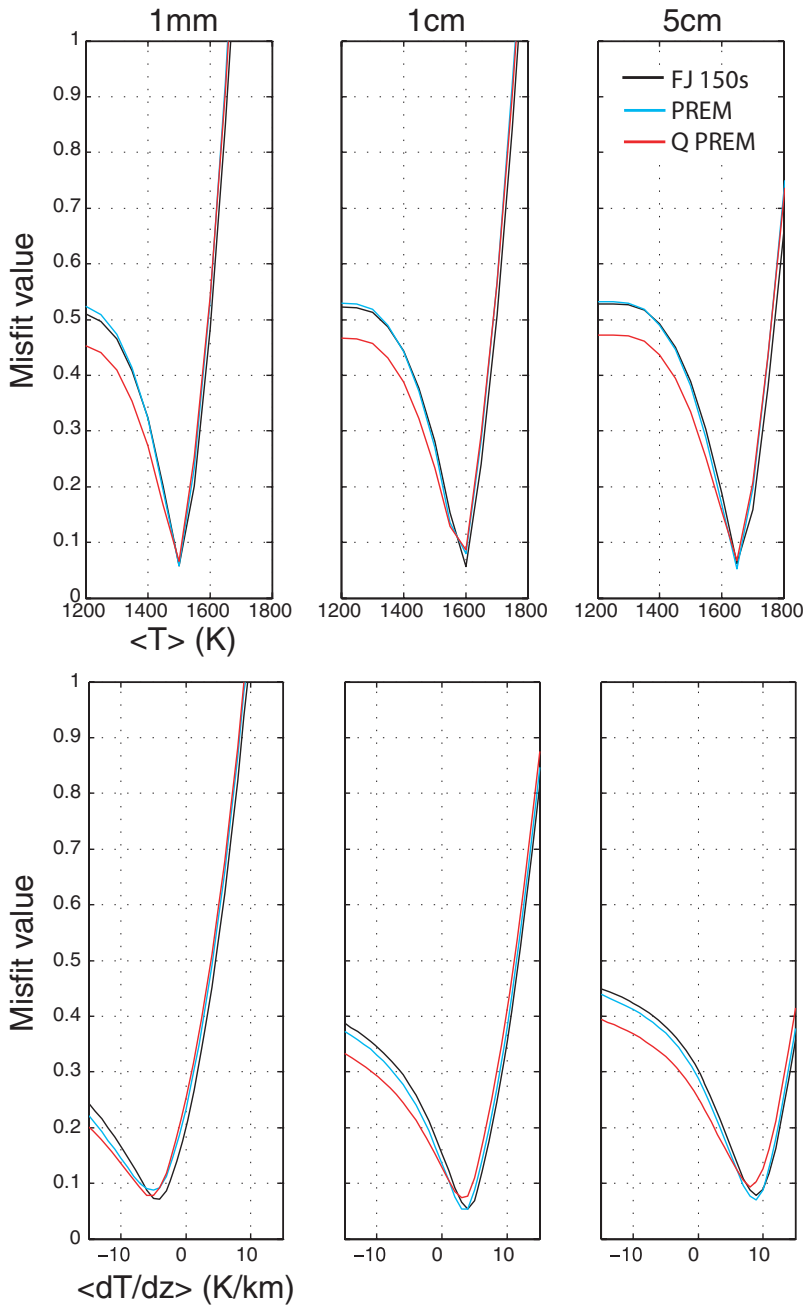

Figure 8. Misfit values for isotherms (top panels) and linear thermal structures assuming $T_{\mathrm{REF}}(100\,\mathrm{km}) = 550$ K (bottom panels) at given constant grain sizes. Same cases of Fig. 7. Predictions for isotherms at 1600 K and GS = 1 cm are on Fig. S3 of the supporting information.

different background model does not introduce any modification to the radial attenuation profiles, but it affects the predictions as a function of angular order, according to the computed eigenfunctions of the models. As illustrated in Fig. 7, the predictions, when using the two different background models, show notable systematic differences. Fundamental modes at high angular order ($\ell >$ 60 for ${}_0S$ and $\ell > 30$ for ${}_0T$) are affected. For the same best-fit physical structure, the model with PREM background fits better the ${}_0T$ observations up to $\ell = 60$, but the model with iPREF as background fits better the (few) data at higher ℓ and fits better the data for ${}_0S$ at any ℓ. On the whole, the effects on interpretation are also not significant in this case (Fig. 8). Nevertheless, it is important, in our opinion, to take into account this effect whenever new models of radial seismic attenuation are constructed. As stated earlier, we prefer to use iPREF for our physical interpretation. We explain the reasons in the next section. In addition, we note that both PREM and iPREF have radial anisotropy in the shallow part of the mantle, to fit both Love (${}_0T$) and Rayleigh (${}_0S$) wave dispersion. We tested the effect of using an isotropic model instead, and it is negligible. Finally, because the two reference models are dispersive, there is also a dependence of the computed eigenfunctions on their attenuation profiles. We tested that this is very small compared with the elastic part of the models and can be neglected as well.

Finally, we show how shallow structure affects interpretation. The attenuation values presented in the previous section have been computed by assuming a thermally conductive lid at the top.

Therefore, according to the strong temperature dependence of the physical model, we obtained very low attenuation values in the shallow part of the mantle (e.g. see Fig. 6). On the other hand, observations, which are sensitive to the real 3-D Earth structure, show, overall, higher values. Seismic reference models, indeed, are characterized by relatively higher values in the top of the mantle (Fig. 1 or 6). In Fig. 7, we compare the predictions by substituting the values predicted from the 1-D thermal structure in the top 80 km, with a uniform layer at $Q_S = 300$. According to the different depth sensitivity, high ℓ toroidal mode observations are more affected than spheroidal (Fig. 7). This affects slightly the interpretation (Fig. 8). The shallow attenuation structure trades-off with structure around 100 km. Consequently, the physical models, which are able to fit (i.e. misfit <0.05) surface wave observations satisfactorily, have attenuation values more similar to QL6 around 100 km (see Fig. S4(d), in the supporting information).

Why is iPREF preferable?

Seismic reference models are constructed to provide a satisfactory fit to global seismic data. The two most commonly used global models are the AK135 model (Kennett *et al.* 1995) and the PREM model (Dziewonski & Anderson 1981). AK135 is based on the inversion of teleseismic traveltimes from the ISC catalogue. It is characterized by continental lithospheric structure and provides poor constraints on the average structure of the upper mantle, consistent with the data coverage, which is biased towards continents. PREM includes fundamental and overtone long period mode data, therefore, is more sensitive to the average upper-mantle (shear) seismic structure. Radial anisotropy was required to fit together fundamental spheroidal and toroidal mode dispersion. It includes a limited set of traveltimes as well. Parametrization of PREM included a large discontinuity at 220 km, which appears not required by data (e.g. Shearer 1996). PREM is a very good seismic reference model for upper-mantle average structure, and from a purely seismic point of view, there is no need to look for an alternative model for interpretation of long-period data. Seismic models are, however, not directly interpretable in terms of temperature and composition (see Cammarano *et al.* 2003) because they are not required to have a physical meaning. For example, the large discontinuity at 220 km imposed in PREM is not reconcilable with simple mineral physics models (Cammarano *et al.* 2003). Recently, we obtained a 3-D V_S model, based on the inversion of long-period data by starting from a physical reference model (one of the adiabatic pyrolitic models PREF, obtained in the previous work of one of us; Cammarano *et al.* 2005). The resulting average model (iPREF, see the supporting information) fits normal-mode data, as well as PREM and better than PREF. The model does not have the 220 km discontinuity that, hence, does not appear required by long-period data, and it is well constrained except near upper-mantle discontinuities (Cammarano & Romanowicz 2007).

Although both PREM and iPREF obtain a satisfactory fit for global seismic data (e.g. fundamental modes and first-order overtones), we tend to favour iPREF, as this is inverted from a physical reference model (an adiabatic pyrolite). The elastic and anelastic properties as a function of pressure, temperature and composition for this model are uniquely determined (see Cammarano & Romanowicz 2007), and therefore, iPREF has a clear meaning in terms of temperature and/or composition. Because the effects on the interpretation of attenuation measurements are not large, as shown in the previous section, our choice is not particularly relevant to this paper. However, it is useful to keep in mind that the search for physical structure (temperature, composition and grain size) fitting seismic data should be based on available mineral physics knowledge on elastic and/or anelastic properties of mantle minerals. In this paper, we focus exclusively on global measurements of attenuation, but the approach is very general and can benefit from the integration of different seismic data.

3.2.2 Sensitivity to model parameters

In Fig. 9, we show the effects on interpretation of the reference period and the activation volume chosen in the Faul & Jackson's model. In our standard FJ-150s model, we used a reference period of 150 s to compute the radial attenuation profile. When we reduce the reference period to 75 s, which is close to the limit of a typical surface wave band, interpretation in terms of temperature and grain size slightly changes (Fig. 9). At a given grain size, a 50 K (or less) colder $\langle T \rangle$ is required or a 0.2 K km^{-1} larger thermal gradient, when starting with a given reference temperature at 100 km. Choosing a longer reference period will give opposite results. More important are the effects of activation volume. At low V^*, observations are best fit with a relatively colder upper mantle or with a strongly negative thermal gradient when starting from a $T_{\rm REF}(100\,{\rm km})$=1550 K (Fig. 9). In the latter case, we obtain that, for the low V^* tested (i.e. 6×10^{-6} m^3 mol^{-1}), only the less negative thermal gradient (-0.1 K km^{-1}), associated with a larger grain size (5cm) is able to predict the correct shape required by high ℓ observations, derived from surface wave studies (Fig. 10). In contrast, at high activation volume (20×10^{-6} m^3 mol^{-1}), we find that when starting from 1550 K at 100 km, only the model with small grain size (1 mm) and less positive thermal gradient (though still 1 K km^{-1}!) is able to reproduce well the whole range of observations (Fig. 10). It is worth pointing out that for our standard case ($V^* = 12 \times 10^{-6}$ m^3 mol^{-1}), only the physical structure with *GS* of 1 cm, associated with a dT/dz of 0.4 K km^{-1} between 100 and 400 km, fits the data well at high ℓ, whereas at small or large *GS*, the fit is not as good (Fig. 10).

As previously discussed, the activation volume for a given mechanism is expected to decrease, but not dramatically, with pressure. Following the procedure given earlier, we tested that the effects are not significant compared with the effects of varying the absolute value of V^* (Fig. 9). Decreasing V^* with depth helps to smooth the curvature of radial attenuation profiles, however, consistent with observations that are sensitive to deeper structure.

4 EFFECTS OF WATER

The mechanisms observed by Faul & Jackson (2005) refer to melt-free and dry olivine. Including water in nominally anhydrous minerals (as olivine) has been shown to affect rheology significantly (and electrical conductivities as well; for a recent review on both effects, see Karato 2006a). Even a trace amount of water weakens olivine and olivine-rich rocks significantly (e.g. Mei & Kohlstedt 2000; Karato & Jung 2003). Theoretically, this can be explained by the role of hydrogen in enhancing the kinetics of defect motion (for more details, see Karato 2006a; Kohlstedt 2008). A similar behaviour has been predicted also for viscoelastic relaxation at seismic frequencies (Karato 1995). In general, it is reasonable to assume that $Q^{-1} \propto W^{\alpha r}$, where Q^{-1} is attenuation (i.e. $1/Q_S$), W is the water content, α is the frequency dependence and r is a constant that depends on the process. The value of this constant has been estimated between $\sim$1, for dislocation mechanisms, and $\sim$2, in case of grain boundary mechanisms (Karato 2006b). To model the water effects, we consider an additional, positive contribution to the dry

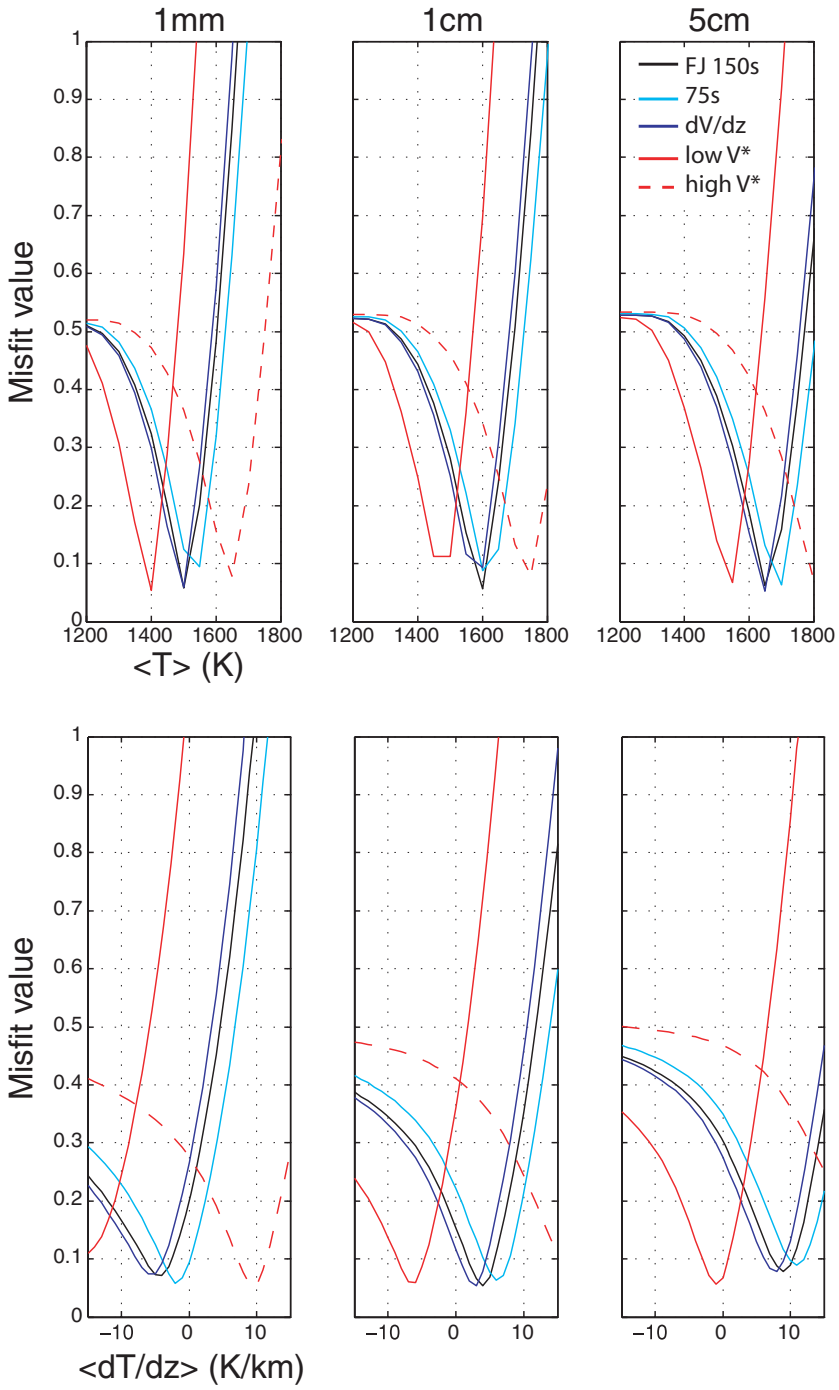

Figure 9. Misfit values for isotherms (top panels) and linear thermal structures assuming $T_{\mathrm{REF}}(100\,\mathrm{km})$=1550 K at given constant grain sizes. Black curve (FJ, 150 s) is the regular Faul & Jackson model at a reference period 150 s, light blue (75 s) is for a reference period of 75 s, blue ($\mathrm{d}V^*/\mathrm{dz}$) is decreasing V^* with depth, following the instructions given in the text, red (low V^*) is assuming a constant $V^* = 6 \times 10^{-6}\,\mathrm{m^3\,mol^{-1}}$, dashed red (high V^*) is with $V^* = 20 \times 10^{-6}\,\mathrm{m^3\,mol^{-1}}$.

attenuation. We define the total attenuation as

$$Q^{-1} = Q^{-1}_{\mathrm{dry}}(P, T, d, \omega) + Q^{-1}_{\mathrm{wet}}(P, T, W), \tag{5}$$

where Q^{-1}_{dry} is here assumed to be the Faul & Jackson value and Q^{-1}_{wet} is the water contribution. The reason for using expression (5) is to preserve the knowledge of the T and grain-size dependence of the Faul & Jackson's model for dry olivine and include an empirical correction for water, based on recent experimental results at high temperature (Aizawa *et al.* 2008). In spite of large uncertainties, we know that this correction is always positive (higher attenuation, see Fig. 11a). The effects on pressure due to the added water must be also considered. Therefore,

$$Q^{-1}_{\mathrm{wet}}(P, T, W) = A(T, P)W^{\alpha r}, \tag{6}$$

where α is assumed to be the one from Faul & Jackson (i.e. 0.27). The temperature dependence at low pressure (0.2 GPa) of Q^{-1}_{wet} is estimated on the basis of the Aizawa's experiments (Aizawa *et al.* 2008). We compared the T-dependent attenuation for two natural

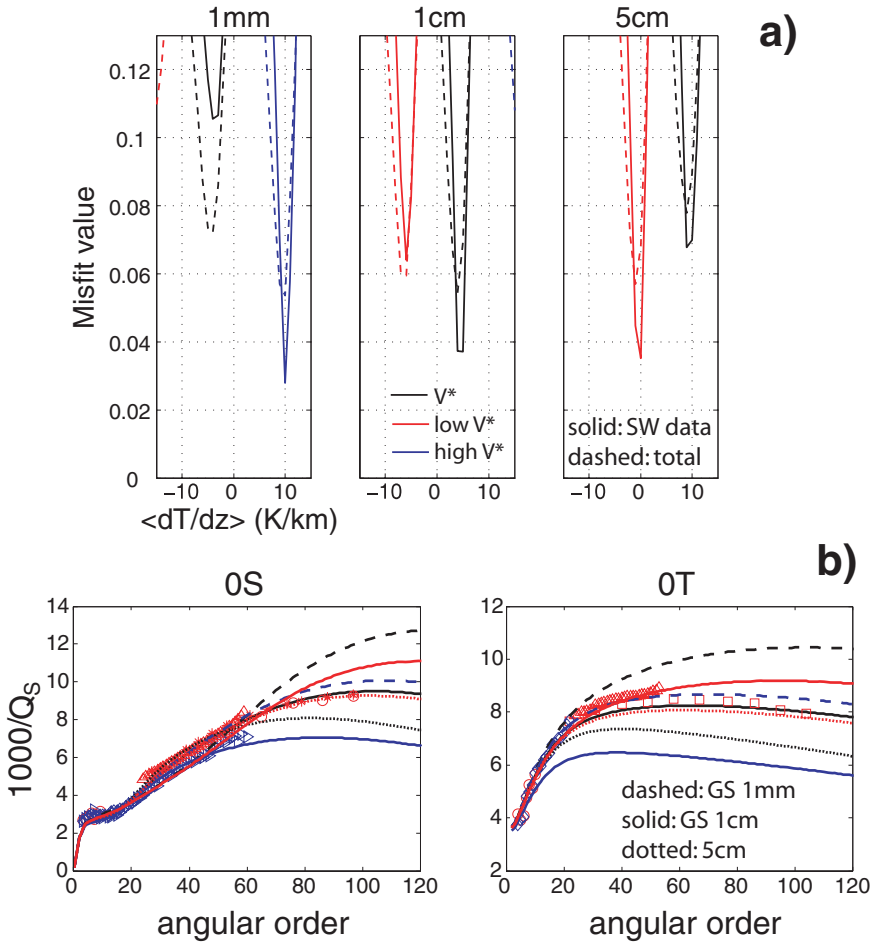

Figure 10. (a) Best fitting models (misfit value <0.13), assuming low, standard or high V^* (values as in Fig. 9) for three constant grain sizes. Dashed are total misfit, solid lines are for observations based on surface wave studies. (b) Predictions of best-fit models of panel a. Dashed are at 1mm grain size, solid at 1 cm and dotted at 5 cm. Colour scheme for different V^* is the same of panel a.

dunite samples, which are characterized by a different amount of water (Fig. 11a). The 'wet' sample retains, probably, the entire inventory of water (∼2 wt per cent) during the high-T experiments, including 0.0187 wt per cent of molecular water. The 'dry' sample, conversely, has lost most of the water and behaves similar to anhydrous material (Fig. 11). The effect of water to enhance viscoelastic relaxation processes has been clearly observed for the first time with these experiments. However, a precise formalism of the water dependence on solid-state viscoelastic relaxation is hampered because of the structural (and compositional) complexity of the natural samples, the marginal, but not negligible, role of partial melt and, last but not the least, the role of the fluid phase (Aizawa *et al.* 2008). Further studies on simpler material will better characterize the effect of water. At the moment, we can use the available indications to give a brute estimate of the possible water effects on absolute Q^{-1}. The difference in observed attenuation between the 'dry' and 'wet' (saturated) sample increases exponentially with temperature, consistently with an enhanced activated process. Often, a typical Arrhenius relationship, that is, $A(T, P_0) = B \exp(-E^*_W/RT)$, where E^*_W is the contribution to the activation energy due to water, is used to model activated processes. To fit Aizawa's data, we found an exponential dependence to T of the pre-exponential term (B), assuming a value of $E^*_W = 50\,\mathrm{kJ\,mol^{-1}}$ (Karato & Jung 2003). Because of the several factors that contribute to the total behaviour and their relative importance as temperature varies, we do not give any physical explanation for this 'non-Arrhenius' behaviour. It is useful to note, however, that water solubility increases as function of T at low pressure (Zhao *et al.* 2004) and the effects related to solid-state viscoelastic relaxation are, thus, expected to be more enhanced as temperature increases. Note, however, that the opposite should be true at high pressure (>6 GPa), where water solubility decreases with T (Bolfan-Casanova *et al.* 2007).

Pressure effects can be modelled by multiplying $A(T, P_0)$ with the exponential factor $\exp(PV^*_W/RT)$, where V^*_W is the contribution to activation volume due to water content. Note that P dependence of the dry case is already included in attenuation predicted with the Faul & Jackson's model. In absence of direct constraints on V^*_W, we rely again on information from rheology. Using a value of $V^*_W = 1.06 \times 10^{-5}\,\mathrm{m^3\,mol^{-1}}$ (Kohlstedt *et al.* 1996), we obtain that attenuation for a constant 0.01 wt per cent water is much larger than for the dry case, both at low and high pressure (Fig. 11b). With this constant amount of water and the described P–T dependent model, we do not find any attenuation profile that is able to fit the data satisfactorily at any reasonable T and GS profile. For example, assuming isothermal structures for given grain sizes, we found that the best-fit model always has a value >0.13 for surface wave observations (Fig. 12). This is due to the very high values

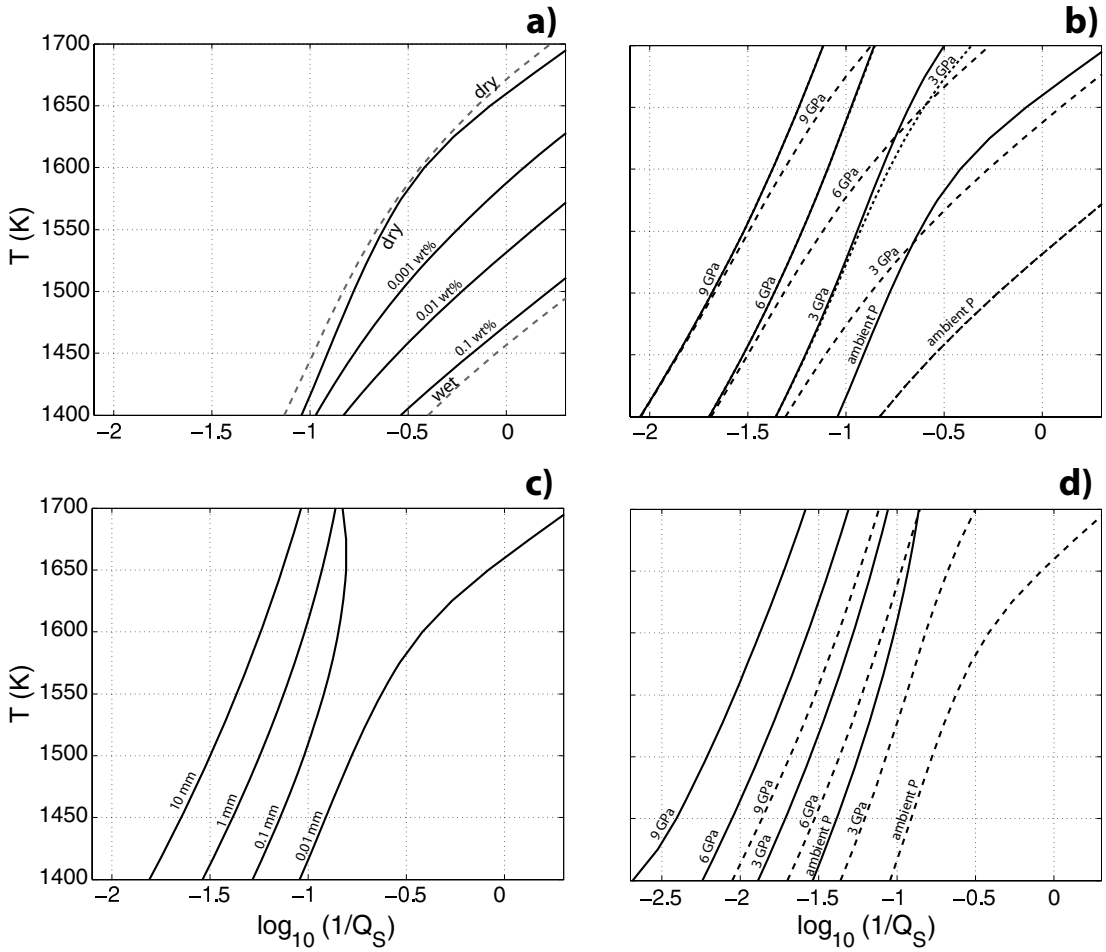

Figure 11. Modelled water effects on P-T-dependent attenuation. (a) T-dependent attenuation as function of water content at ambient P, period = 150 s and for a given GS of 0.01 mm (solid lines). The 'wet' and 'dry' samples (dashed lines) are, respectively, the attenuation values for two natural dunite samples (1093 and 1066 of Aizawa *et al.* 2008). The original laboratory data have been interpreted with the Burgers model (same formalism of Faul & Jackson 2005) but, in this case, without the (unconstrained) grain size deependence. Both samples have an average grain size around 0.02 mm. (b) Modelled T-dependent attenuation at different pressures for dry case (solid) and with 0.01 wt per cent water, period = 150 s and grain size of 0.01 mm. Dashed lines are for $V^*_W = 1.06 \times 10^5$ m^3 mol−1. Dotted are with $V^*_W = 2.4 \times 10^5$ m^3 mol^{-1}. For comparison, panels (c) and (d) show, respectively, variations of Q^{-1} with grain size and effects of pressures for two given grain sizes (solid lines for 1mm and dashed for 0.01 mm) computed with the Faul & Jackson's model at period of 150 s. See also Fig. S5 in the supporting information.

of attenuation around 100 km. When using a much large activation volume ($V^* = 2.4 \times 10^{-5}$ m^3 mol^{-1}), we find that interpretation in terms of average T does not change much (Fig. 12). However, only models with $GS \leq 1$ mm and $< T > = 1500$ K, are able to obtain a similar fit as in the dry case (Fig. 12). In this case, Q^{-1} values at 100 km (3 GPa) are sensibly lower than before and values at higher P are very similar to the dry case (see Fig. 11b). We point out that our 'water-contribution' to Q^{-1} is independent of grain size, but it does become larger as temperature increases. For example, at a given 1 cm GS and assuming isothermal structure, a $\langle T \rangle = 1600$ K is required for both dry and 0.01 wt per cent wet case. However, values of Q^{-1} for the wet case are significantly higher, especially at shallow depth, and the misfit is not as good as the dry case (Fig. 12). On the other hand, for a given 1 mm GS, seismic observations are best explained with a 1500 K isotherm. In this case, the profiles between dry and wet are more similar, as effect of water on absolute attenuation are less important at lower temperature.

Finally, we note that when modelling water effects, we should consider the feedback with all the other parameters and not only with P and T. We decided to neglect the effect of water on frequency dependence. The Aizawa's experiments seem to support such an assumption, not showing any systematic variation of α with water content. In particular, the 'wet' sample has a very similar frequency dependence (∼0.26) to the Faul & Jackson's value. We also assume that there is no feedback between the grain-size dependence and water dependence.

5 CONSTRAINTS OF THE PHYSICAL STRUCTURE OF THE UPPER MANTLE

The lack of knowledge of the absolute value of activation volume seriously limits the interpretation of seismic attenuation measurements. Yet, it is possible to test plausible physical models against these data, deriving what are the associated physical structures, which fit the observations. Adding independent constraints on temperature (plus grain size and water content) may help to discriminate between them and therefore inform us on the physical model that is compatible with the combined observations. At the same time, the physical structure of the mantle will be better constrained as

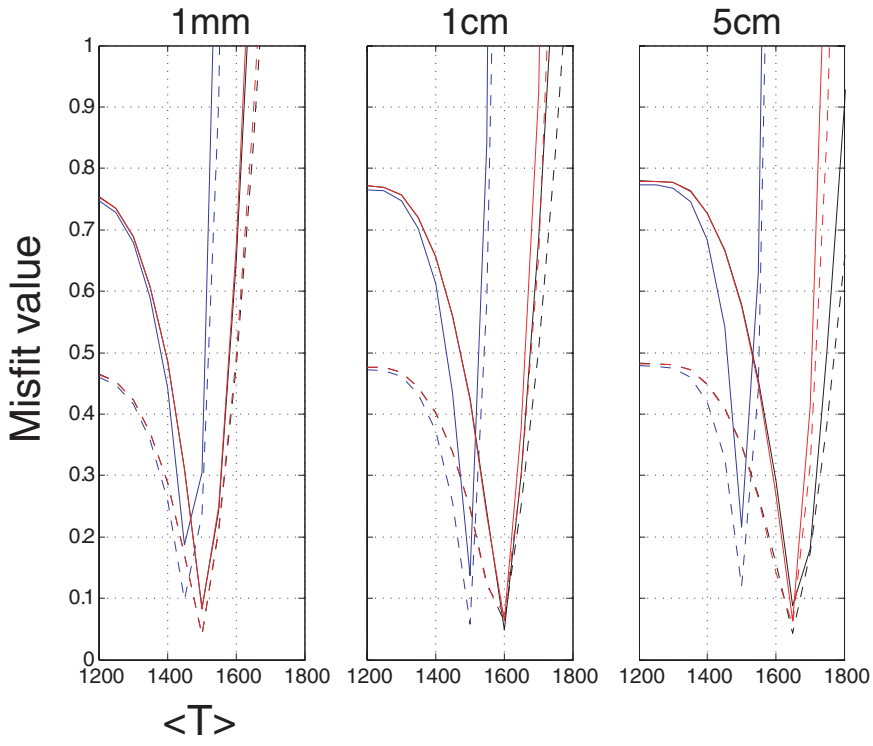

Figure 12. Misfit values for isotherms at given constant grain sizes for surface wave (solid) and free-oscillations (dashed) observations. Black is the dry case (FJ, 150 s, as in Fig. 7), blues is with 0.01 wt per cent of water with $V_W^* = 1.06 \times 10^5$ m^3 mol^{-1} and red is for the same amount of water and $V_W^* = 2.4 \times 10^5$ m^3 mol^{-1}.

well. For example, we have seen that giving reference temperatures based on independent constraints at 100 km, helps to relate specific best-fit *T-GS* structures for each physical model tested.

Interpretation may be further refined when available information on radial seismic velocity profiles, for example, iPREF, is coupled to the attenuation data. The interpretation of models like iPREF (Cammarano & Romanowicz 2007) or a simple visual inspection of the iPREF model (supporting information), is already providing the direction of the expected results. For example, the high gradient of V_S required by long period waveforms between 250 and 350 km is clearly not consistent with a very positive thermal gradient.

As we will mention in the discussion, we prefer to adopt a more robust approach, based on a 3-D analysis of seismic waveforms in terms of temperature (and grain size) and composition, including water. We will present the results of such an analysis in a separate paper. We anticipate, however, that the current knowledge of elastic and anelastic properties of upper-mantle minerals is sufficient to get insights on the average physical structure of the upper mantle and to give better constraints on uncertain physical parameters such as activation volume.

Finally, we would like to draw attention on whether the physical structures related to a given physical model are dynamically feasible. From a qualitative point of view, a negative thermal gradient or a highly positive thermal gradient appear incompatible with dynamic models. In general, dynamic models will not only improve our constraints on current physical conditions of the Earth's interior but are also an essential tool to understand the evolution of the Earth's internal processes. It is desirable that future cross-disciplinary studies use a consistent physical hypothesis for providing parameters for models as well as interpretation of seismic (and other geophysical) data. For example, the pressure, temperature and composition dependence of the elastic properties should be the same, as well as the pressure dependence for rheology and seismic attenuation.

Such an approach will help to test whether given values of unknown or uncertain material properties at high pressure and high temperature are consistent with observations and dynamic evolution or not.

6 DISCUSSION

In this paper, we are concerned with the physical meaning of seismic attenuation within the Earth. The experimental model used, represents the state-of-the-art knowledge of viscoelastic relaxation at seismic frequencies for relevant mantle minerals. Unfortunately, experimental conditions and materials are not similar to expected mantle conditions. Therefore, one may ask: is the mechanism observed in the laboratory experiments relevant to the Earth's upper mantle? If so, is it stable down to 400 km? Or is it replaced by a different mechanism at a certain depth?

As discussed previously, Faul & Jackson's experiments found evidence for a diffusive GBS mechanism, governing seismic attenuation. Diffusion along grain boundaries is a preferred shortcut for diffusive processes, and therefore, activation volume is expected to be higher than for 'purely' diffusive processes. In general, there is some controversy on the plausibility of GBS at high pressures. For example, the high V^* that characterizes GBS mechanisms implies a larger and larger activation enthalpy as pressure increases and, eventually, the 'shutdown' of the process. It is possible, as for the deformation regimes, to think about a change with depth in the dominant physical mechanisms for seismic intrinsic attenuation. Note, however, that the pressure effects could be counter-balanced by the coarser grain sizes expected in the upper mantle (mm to cm scale)

compared with the experimental ones (μm to mm scale). Hence, it is plausible that the mechanism observed by Faul & Jackson may also occur at larger pressures for the expected larger grain sizes of the upper mantle. It is important to note that if the physical mechanism does not change with depth, the activation volume is theoretically expected to decrease, but slightly, along the upper mantle.

In addition to temperature, grain size and water, there are several other parameters that can have a direct (e.g. dislocations) or indirect (e.g. compositional effects on water solubility) influence on attenuation. The viscoelastic response at seismic frequencies for a polyphase, polycrystalline material is, indeed, due to a complex interplay among several parameters. There is a long way to go for understanding the processes well enough, and thus, to get a robust formal relation, which includes several key parameters. However, the recent advances are promising to improve knowledge of the processes responsible for seismic attenuation. For example, the role of dislocations will be soon investigated in the laboratory (Ian Jackson, personal communication, 2008). The presence of melt also tends to enhance attenuation, though a precise quantification depends on the structural aspects of the fluid inclusions (Jackson 2008). At the expected T and GS at ∼100 km, the solid state mechanism observed by Faul & Jackson already gives high attenuation values (e.g. see Fig. 6). And the presence of water will tend to even increase such high values. Uncertainties in pressure dependence certainly preclude us from making conclusive statements. Based on the available knowledge, we can speculate, however, that there is no need to invoke the secondary effects of partial melt to explain seismic attenuation at a global scale.

In addition, it is unknown whether the measured attenuation of seismic data is affected significantly by scattering effects or by not appropriately modelled focusing and defocusing effects. The correspondence with tectonics of attenuation structures emerging from available 3-D attenuation models (low 1/Q beneath continents and high 1/Q beneath oceans at shallow depth) indicates that we are probably observing intrinsic attenuation effects. However, in theory, it is possible for *ad hoc* (fractal) geometries of 3-D heterogeneity to reproduce the whole set of attenuation observations, with scattering effects only (van der Baan 2002). Although unrealistic, this example highlights the necessity to account somehow for the role of scattering. In particular, we found it interesting that complexities at any scale would be able to explain the low frequency dependence that characterizes seismic wave propagation within the absorption band.

Modelling and correcting for focusing effects at long periods is in principle less problematic, but the 3-D elastic structure should be well known, as well.

In summary, the advances in experimental and computational mineral physics, seismic observations and their simulations, geochemistry, petrology and geodynamic modelling will certainly contribute to constantly improve our knowledge. However, integrating the current information can already partially answer the above questions and guide future research.

In this paper, we focused on the simple radial interpretation of attenuation measurements. We showed that attenuation data are useful, when combined with independent constraints, to constrain the thermal state of the upper mantle. Although we provide models that have a physical meaning and provide a satisfactory fit to the seismic attenuation data, obtaining an average attenuation structure for the Earth's upper mantle is beyond the scope of this work. In fact, a consistent thermal (and compositional) interpretation should account, at the same time, for both attenuation and seismic velocity. In other words, from the point of view of fitting seismic waveforms, we should be able to fit the full waveforms and obtain a 3-D attenuation model that is compatible with seismic observations. Note that account for 3-D effects is paticularly important in consideration of the non-normal distribution and the large range of variations in attenuation expected in the upper mantle. Due to non-linearity of attenuation and seismic velocity with temperature (and water content) and the effects of 3-D elastic structure that can mask intrinsic attenuation, it is clearly important to perform an accurate 3-D analysis. This study, together with our previous inversion of long-period seismic waveforms for temperature (Cammarano & Romanowicz 2007), provides the basis for such complete waveform analysis that will be the subject of our future work.

An effort to combine the different pieces of information together should, eventually, also better address other more general questions, related to the one here discussed, such as: is there a dominant scale of heterogeneity in the Earth's mantle? If so, which one? Is the mantle convecting as a whole? Or to what extent does the 660 km discontinuity act as a barrier to mantle convection?

7 CONCLUSIONS

A physical interpretation of global measurements of seismic attenuation has the potential to inform us on average thermal structure of the upper mantle. Using a given physical model, based on available experiments of seismic attenuation (i.e. the Faul & Jackson's model for dry olivine), we found that simple thermal (and grain size) structures are able to fit observations similarly to seismic models. In contrast to seismic models, layered parametrization is not needed here. Instead, our parametrization relies on current knowledge of pressure, temperature and grain size dependence of seismic attenuation derived from laboratory experiments. The models do not have any sharp gradients below 100 km, which are not required to fit the data used.

Uncertainties in the physical model, in particular the unknown pressure effect, hamper a clear interpretation of the seismic attenuation measurements. Nevertheless, adding independent constraints on temperature, grain size and water content, constrains well the physical structures that are associated with a given physical hypothesis and help to reduce uncertainties on the pressure dependence of attenuation (i.e. V^*). For example, starting from a temperature of 1550 K at 100 km and assuming that the seismic attenuation is governed by the Faul & Jackson's mechanism, we found that negative thermal gradients associated with several cm grain sizes (assuming low V^*) or an approximately adiabatic gradient associated with ∼1 cm grain size are possible. Higher values of V^* would require strongly positive thermal gradients that are not compatible with the high V_S gradient, which characterizes global seismic models. Water enhances attenuation and trade-offs with temperature. Based on the available constraints, it is likely that water will have a secondary effect on global attenuation measurements.

A combined seismic analysis, based on modelling together elastic data of mantle minerals and anelasticity as a function of pressure, temperature (and grain size) and composition (including water), promises to exploit most of the information contained in the seismic data. The full waveforms can thus be analysed and the contributions on phase (mostly related to the elastic part) and amplitude (mostly related to anelasticity) can determine the (3-D) physical structure (i.e. T–C), which is consistent with the physical model (and parameters) tested.

ACKNOWLEDGMENTS

We thank Uli Faul and Ved Lekic for useful discussions. We also thank David Kohlstedt and Ian Jackson for sending us pre-prints of their papers. We further thank Jeannot Trampert, Joe Resovsky and an anonymous reviewer for their constructive reviews. This paper has been supported by the NSF grant EAR0456335. This is the BSL contribution n. 08-03.

REFERENCES

Aizawa, Y., Barnhoorn, A., Faul, U., Gerald, J.F. & Jackson, I., 2008. The influence of water on seismic wave attenuation in dunite: an exploratory study, *J. Petrol.,* **49,** 841–855.

Anderson, D. & Hart, R., 1978. Q of the earth, *J. geophys. Res.,* **83,** 5869–5882.

Anderson, D. & Minster, J., 1979. Frequency-dependence of q in the earth and implications for mantle rheology and chandler wobble, *Geophys. J. R. astr. Soc.,* **58**(2), 431–440.

Anderson, D., Ben-Menahem, A. & Archambeau, C., 1965. Attenuation of seismic energy in the upper mantle, *J. geophys. Res.,* **70,** 1441–1448.

Berckhemer, H., Kampfmann, W., Aulbach, E. & Schmeling, H., 1982. Shear modulus and q of forsterite and dunite near partial melting from forced oscillation experiments, *Phys. Earth planet. Inter.,* **29,** 30–41.

Bolfan-Casanova, N., Bali, N. & Koga, K., 2007. Pressure and temperature dependence of water solubility in forsterite: implications for the activity of water in the earth's mantle, *Geochemica et coscmochimica acta,* **71,** A106.

Boyd, F. & Meyer, H., 1979. The mantle sample: inclusions in kimberlites and other volcanics, in *Proceedings of the Second International Kimberlite Conference*, **Vol. 2,** p. 423, AGU, Washington, DC.

Cammarano, F. & Romanowicz, B., 2007. Insights into the nature of the transition zone from physically constrained inversion of long-period seismic data, *PNAS,* **104,** 9139–9144.

Cammarano, F., Goes, S., Vacher, P. & Giardini, D., 2003. Inferring upper mantle temperatures from seismic velocities, *Phys. Earth planet. Inter.,* **139,** 197–222.

Cammarano, F., Deuss, A., Goes, S. & Giardini, D., 2005. One-dimensional physical reference models for the upper mantle and transition zone: combining seismic and mineral physics constraints, *J. geophys. Res.,* **110**(B01306), doi:10.1029/2004JB003272.

Cobden, L., Goes, S. & Cammarano, F., 2008. Thermo-chemical interpretation of one-dimensional seismic reference models for the upper mantle: evidence for bias due to heterogeneity, *Geophys. J. Int.,* in press.

Derby, B. & Ashby, M., 1987. On dynamic recrystallisation, *Scripta Metallurgica,* **21,** 879–884.

Deschamps, F., Snieder, R. & Trampert, J., 2001. The relative density-to-shear velocity scaling in the uppermost mantle, *Phys. Earth planet. Inter.,* **124,** 193–211.

Deschamps, F., Trampert, J. & Snieder, R., 2002. Anomalies of temperatures and iron in the uppermost mantle inferred from gravity data and tomographic models, *Phys. Earth planet. Inter.,* **129,** 245–264.

Dijkstra, A., Drury, M., Vissers, R., Newman, J. & Roermund, H.V., 2004. Shear upper mantle: evidence from alpine- and ophiolite-type peridotite massif, in *Flow processes in faults and shear zones*, **Vol. 224,** pp. 11–24, eds Alsop, G.I., Holdsworth, R.E., McCaffrey, K.J.W. & Hand, M., Geol. Soc. London Spec. Publication.

Durek, J. & Ekström, G., 1996. A radial model of anelasticity consistent with long period surface-wave attenuation, *Bull. seism. Soc. Amer.,* **86,** 144–158.

Dziewonski, A. & Anderson, D., 1981. Preliminary reference earth model, *Phys. Earth planet. Inter.,* **25,** 297–356.

Faul, U. & Jackson, I., 2005. The seismological signature of temperature and grain size variations in the upper mantle, *Earth planet. Sci. Lett.,* **234,** 119–134.

Faul, U., Gerald, J.F. & Jackson, I., 2004. Shear-wave attenuation and dispersion in melt-bearing olivine polycrystals. part ii: Microstructural interpretation and seismological implications, *J. geophys. Res.,* **109**(B06202), doi:10.1029/2003JB002407.

Forte, A. & Mitrovica, J., 2001. Deep-mantle high viscosity flow and thermochemical structure inferred from seismic and geodynamic data, *Nature,* **410,** 1049–1056.

Frost, H. & Ashby, M., 1982. *Deformation-Mechanism Maps: The Plasticity and Creep of Metals and Ceramics*, 166 pp. Oxford: Pergamon Press.

Goes, S., Govers, R. & Vacher, P., 2000. Shallow mantle temperatures under Europe from *P*- and *S*-wave tomography, *J. geophys. Res.,* **105,** 11 153–11 169.

Gribb, T. & Cooper, R., 1998. A high temperature torsion apparatus for the high-resolution characterization of internal friction and creep in refractory metals and ceramics: application to the seismic-frequency, dynamic response of Earth's upper mantle, *Rev. Sci. Instrum.,* **69,** 559–564.

Hirschmann, M., 2000. Mantle solidus: experimental constraints and the effects of peridotite composition, *Geochem. Geophys. Geosyst.,* **1,** doi: 10.1029/2000GC000070.

Hirth, G. & Kohlstedt, D., 1996. Water in the oceanic upper mantle: implications for rheology, melt extraction and evolution of the lithosphere, *Earth planet. Sci. Lett.,* **144,** 93–108.

Jackson, I., 2000. Laboratory measurements of seismic waves dispersion and attenuation: recent progress, in *Earth's deep interior. Mineral Physics and Tomography from the Atomic to the Global Scale*, pp. 265–289, ed. Karato, S., AGU.

Jackson, I., 2008. Properties of rocks and minerals - physical origins of anelasticity and attenuation in rock, in *Treatise on Geophysics*, Elsevier, Amsterdam.

Jackson, I. & Paterson, M., 1993. A high-pressure, high-temperature apparatus for studies of seismic wave dispersion and attenuation, *Pageoph,* **141,** 445–466.

Jackson, I., Gerald, J.F., Faul, U. & Tan, B., 2002. Grain-size-sensitive seismic wave attenuation in polycrystalline olivine, *J. geophys. Res.,* **107,** doi:10.1029/2001JB001225.

Jacobsen, S. & Smyth, J., 2006. Effects of water on the sound velocities of ringwoodite in the transition zone, in *Earth's Deep Water Cycle*, pp. 131–145, eds Jacobsen, S. & van der Lee, S., AGU Monograph.

Karato, S., 1993. Importance of anelasticity in the interpretation of seismic tomography, *Geophys. Res. Lett.,* **20,** 1623–1626.

Karato, S., 1995. Effects of water on seismic wave velocities in the upper mantle, *Proc. Japan Academy,* **71,** 61–66.

Karato, S., 1998. A dislocation model of seismic wave attenuation and micro-creep in the earth: Harold Jeffreys and the rheology of the solid earth, *Pageoph,* **153,** 239–256.

Karato, S., 2006a. Influence of hydrogen-related defects on the electrical conductivity and plastic deformation of mantle minerals: a critical review, in *Earth's Deep Water Cycle*, pp. 113–130, eds Jacobsen, S. & van der Lee, S., AGU, Washington DC.

Karato, S., 2006b. Remote sensing of hydrogen in earth's mantle, *Rev. Mineral. Geochem.,* **62,** 343–375.

Karato, S. & Jung, H., 2003. Effects of pressure on high-temperature dislocation creep in olivine, *Phil. Magazine,* **83**(3), 401–414.

Katsura, T. & Ito, E., 1989. The system mg_2sio_4-fe_2sio_4 at high pressures and temperatures: precise determination of stabilities of olivine, modified spinel, and spinel, *J. geophys. Res.,* **94,** 15 663–15 670.

Katsura, T. *et al.*, 2004, Olivine-wadsleyite transition in the system $(Mg, Fe)_2SiO_4$, *J. geophys. Res.,* **109**(B02209), doi:10.1029/2003JB002438.

Kennett, B., Engdahl, E. & Buland, R., 1995. Constraints on seismic velocities in the earth from travel times, *Geophys. J. Int.,* **122,** 108–124.

Keyes, R., 1963. Continuum models of the effect of pressure on activated processes, in *Solids Under Pressure*, pp. 71–91, eds Paul, W. & Warshauer, D., McGraw Hill, New York.

Kohlstedt, D., 2008. Constitutive equations, rheological behavior, and viscosity of rocks, in *Treatise on Geophysics*, Elsevier, Amsterdam.

Kohlstedt, D., Keppler, D. & Rubie, D., 1996. Solubility of water in the α, β and γ phases of $(Mg, Fe)_2SiO_4$, *Contrib. Mineral. Petrol.,* **123,** 345–357.

Lallemant, H.A., Mercier, J., Carter, N. & Ross, J., 1980. Rheology of the upper mantle: inferences from peridotite xenoliths, *Tectonophysics,* **70,** 85–113.

Ledo, J. & Jones, A., 2005. Upper mantle temperature determined from combining mineral composition, electrical conductivity laboratory studies and magnetotelluric field observations: application to the intermontane belt, northern canadian cordillera, *Earth planet. Sci. Lett.,* **236,** 258–268.

Li, L. & Weidner, D., 2007. Energy dissipation at high pressure and high temperature, *Rev. Scientific Instr.,* **78,** 053902.

Li, L., Weidner, D., Ratteron, P., Chen, J., Vaughan, M., Mei, S. & Durham, B., 2006. Deformation of olivine at mantle pressures using the d-dia, *Eur. J. Mineral.,* **18,** 7–19.

Litasov, K., Ohtani, E. & Sano, A., 2006. Influence of water on major phase transitions in the earth's mantle, in *Earth's Deep Water Cycle*, pp. 95–111, eds Jacobsen, S. & van der Lee, S., AGU Monograph.

Matas, J. & Bukowinski, M., 2007. On the anelastic contribution to the temperature dependence of lower mantle seismic velocities, *Earth planet. Sci. Lett.,* **259**(1-2), doi:10.1016/j.epsl.2007.04.028.

McKenzie, D. & Bickle, M., 1988. The volume and composition of melt generated by extension of the lithosphere, *J. Petrol.,* **29,** 625–697.

Mei, S. & Kohlstedt, D., 2000. Influence of water on plastic deformation of olvine aggregates 2: dislocation creep regime, *J. geophys. Res.,* **105,** 21 471–21 481.

Michael, P., 1995. Regionally distinctive sources of depleted morb: evidences from trace elements and h_2o, *Earth planet. Sci. Lett,* **131,** 301–320.

Ohtani, E., Litasov, K., Hosoya, T., Kubo, T. & Kondo, T., 2004. Water transport into the deep mantle and formation of a hydrous transition zone, *Phys. Earth planet. Inter.,* **143-144,** 255–269.

Okal, E. & Jo, B., 1990. Q measurements for phase x overtones, *Pure appl. Geophys.,* **132,** 331–362.

Olgaard, D. & Evans, B., 1988. Grain-growth in synthetic marbles with added mica and water, *Contrib. Mineral. Petrol.,* **100**(2), 246–260.

O'Reilly, S. & Griffin, W., 1987. Eastern australia-4000 kilometers of mantle samples, in *Mantle Xenoliths*, pp. 267–280, ed. Nixon, P., John Wiley and Sons, Chichester.

Poirier, J. & Liebermann, R., 1984. On the activation volume for creep and its variation with depth in the earth's lower mantle, *Phys. Earth planet. Inter.,* **35,** 283–293.

Pollack, H., Hunter, S. & Johnson, J., 1993. Heat flow from the earth's interior: analysis of the global data set, *Rev. Geophys.,* **31,** 267–280.

Raj, R. & Ashby, M., 1971. On grain boundary sliding and diffusional creep, *Metallurgical Transactions*, **2,** 1113–1127.

Resovsky, J., Trampert, J. & van der Hilst, R., 2005. Error bars for the global seismic q profile, *Earth planet. Sci. Lett.,* **230,** 413–423.

Romanowicz, B., 1995. A global tomographic model of shear attenuation in the upper mantle, *J. geophys. Res.,* **100,** 12 375–12 394.

Romanowicz, B. & Durek, J., 2000. Seismological constraints on attenuation in the earth: a review, in *Earth's Deep Interior. Mineral Physics and Tomography from the Atomic to the Global Scale*, pp. 161–179, ed. Karato, S., AGU.

Romanowicz, B. & Mitchell, B., 2008. Q in the earth from crust to core, in *Treatise on Geophysics*, Vol. I, Elsevier, Amsterdam.

Sammis, C., Smith, J. & Schubert, G., 1981. A critical assessment of estimation methods for activation volume, *J. geophys. Res.,* **86,** 10 707–10 718.

Shearer, P., 1996. Transition zone velocity gradients and the 520-km discontinuity, *J. geophys. Res.,* **101**(B2), 3053–3066.

Shito, A. & Shibutani, T., 2003. Nature of heterogeneity of the upper mantle beneath the northern philippine sea, *Phys. Earth planet. Inter.,* **140,** 331–341.

Shito, A., Karato, S., Matsukage, K. & Nishihara, Y., 2006. Towards mapping the three-dimensional distribution of water in the upper mantle from velocity and attenuation tomography, in *Earth's Deep Water Cycle*, pp. 225–236, eds Jacobsen, S. & van der Lee, S., AGU Monograph.

Sipkin, S. & Jordan, T., 1979. Frequency dependence of qscs, *Bull. seism. Soc. Am.,* **69,** 1055–1079.

Smith, M. & Dahlen, F., 1981. The period and Q of the chandler wobble, *Geophys. J. R. astr. Soc.,* **64,** 223–281.

Tan, B., Jackson, I. & Gerald, J.F., 1997. Shear wave dispersion and attenuation in fine-grained synthetic olivine aggregates: preliminary results, *Geophys. Res. Lett.,* **24**(9), 1055–1058.

van der Baan, M., 2002. Constant Q and a fractal, stratified earth, *Pure appl. Geophys.,* **159,** 1707–1718.

van der Meijde, M., Maroen, F. & Giardini, D., 2004. Seismic evidence for water deep in Earth's upper mantle, *Science,* **300,** 1556–1558.

Weertman, J., 1970. The creep strength of the Earth's mantle, *Rev. Geophys.,* **8,** 145–168.

Widmer, R., Masters, G. & Gilbert, F., 1991. Spherically symmetric attenuation within the earth from normal mode data, *Geophys. J. Int.,* **104,** 541–553.

Woodhouse, J., 1988. The calculation of eigenfrequencies and eigenfunctions of the free oscillations of the earth and the sun, in *Seismological Algorithms*, pp. 321–370, ed. Doornbos, D., Academic Press, New York.

Woodhouse, J. & Dahlen, F., 1978. The effect of a general aspherical perturbation on the free oscillations of the earth, *Geophys. J. R. astr. Soc.,* **53,** 335–354.

Yang, Y., Forsyth, D.W. & Weeraratne, D.S., 2007. Seismic attenuation near the east pacific rise and the origin of the low-velocity zone, *Earth planet. Sci. Lett.,* **258,** 260–268.

Zener, C., 1942. Theory of lattice expansion introduced by cold-work, *Trans. Aime,* **147,** 361–368.

Zhao, Y., Frost, D. & Kohlstedt, D., 2004. Solubility of hydrogen in olivine: dependence on temperature and iron content, *Contrib. Mineral. Petrol.,* **147,** 155–161.

APPENDIX

The attenuation as a function of P, T, frequency (ω) and grain size (d) is computed by using the complex compliance, expressed in terms of Laplace transform of the generalized Burgers creep function (after Faul & Jackson 2005)

$$J(t) = J_U \left[1 + \delta \ln J_U + \Delta \int_{\tau_L}^{\tau_H} D(\tau) \left(1 - \mathrm{e}^{\frac{t}{\tau}} \right) \mathrm{d}\tau + \frac{t}{\tau_M} \right], \quad \text{(A1)}$$

where J_U is the unrelaxed compliance, equal to the inverse of shear modulus G_U; $\tau_M (= \mu J_U)$ is the Maxwell relaxation time proportional to the viscosity μ; $\Delta$is the relaxation strength associated with the normalized distribution of anelastic relaxation times $D(\tau) = \alpha \tau^{\alpha-1} / \tau_H^\alpha - \tau_L^\alpha$, with $\tau_L < \tau < \tau_H$ and zero elsewhere, where α is thus the frequency dependence. The temperature and grain-size dependence of the relaxation times is expressed by

$$\tau_i = \tau_{iR} \left(\frac{\mathrm{d}}{\mathrm{d_R}} \right)^m \mathrm{e}^{\left[\left(\frac{\mathrm{E}}{\mathrm{R}} \right) \left(\frac{1}{T} - \frac{1}{T_\mathrm{e}} \right) \right]} \quad \text{(A2)}$$

where τ_i is τ_H, τ_L and τ_M and E is the activation energy. Subscripts R refers to reference values at a reference T (T_R) of 1223 K. The exponent m for the grain-size dependence has different value in case of viscous (τ_M) or anelastic relaxation (τ_H and τ_L). Pressure effects on attenuation have been modelled, though not constrained by data, scaling the relaxation times by exp (PV^*/RT).

The real and imaginary part of the generalized Burgers creep function $J(t)$ are, respectively,

$$J_1(\omega, d, T, P) = J_U(P) \times \left(1 + \delta \ln J_U + \frac{\alpha_Q \Delta}{\tau_\mathrm{H}^{\alpha_Q} - \tau_\mathrm{L}^{\alpha_Q}} \int_{\tau_\mathrm{L}}^{\tau_\mathrm{H}} \frac{\tau^{\alpha_Q - 1}}{1 + \omega^2 \tau^2} \mathrm{d}\tau \right), \quad \text{(A3)}$$

$$J_2(\omega, d, T, P) = J_U(P)\left(\frac{\omega\alpha_Q\Delta}{\tau_{\rm H}^{\alpha_Q} - \tau_{\rm L}^{\alpha_Q}}\int_{\tau_{\rm L}}^{\tau_{\rm H}}\frac{\tau^{\alpha_Q}}{1+\omega^2\tau^2}\,{\rm d}\tau + \frac{1}{\omega\tau_{\rm M}}\right) \tag{A4}$$

and

$$Q_{-1} = J_2(\omega)/J_1(\omega). \tag{A5}$$

The parameters that enter in the equations are given in table 1 of Faul & Jackson (2005). The same formalism, but setting the grain-size dependence (m) to 0 and not modelling pressure effects, is used to fit also the experiments on natural (hydrated) dunite samples (Aizawa *et al.* 2008). Parameters are given in table 2 of Aizawa *et al.* (2008).

A clear explanation of the Burgers model and the derivation of the generalized creep function can be found in the Faul & Jackson's (2005) paper. More details, including the comparison of the Burgers model with alternative one (e.g. the Andrade model) are given in the recent review from Jackson (2008).

SUPPORTING INFORMATION

Additional Supporting Information may be found in the online version of the article.

Appendix S1. This appendix contains (i) iPREF table, (ii) four figures, and (iii) misfit of physical 1-D profiles tested (PDF format).

Please note: Wiley-Blackwell is not responsible for the content or functionality of any supporting information supplied by authors. Any queries (other than missing material) should be directed to the corresponding author for the article.